Sparsity

CosmoStats meets CosmoInformatics

Jason McEwen

http://www.jasonmcewen.org/

Department of Physics and Astronomy
University College London (UCL)

CosmoStats 2013 :: March 2013

Exploiting sparsity
CMB

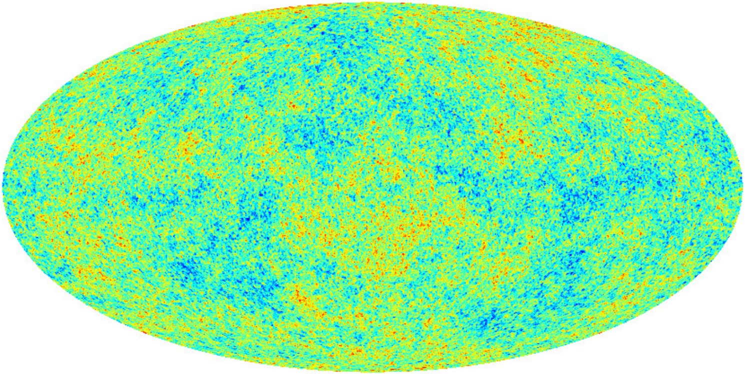

Exploiting sparsity
Wavelet coefficients of CMB

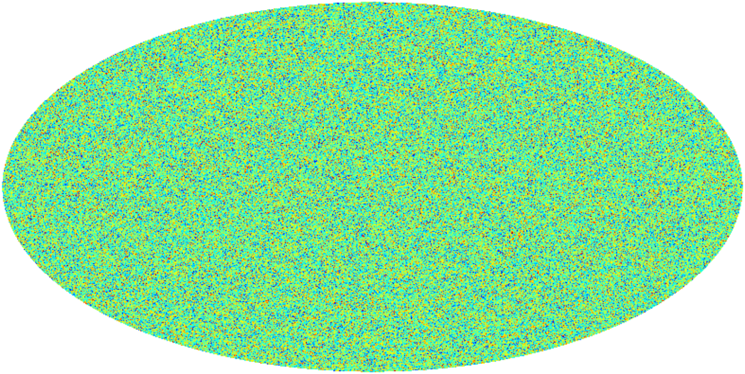

CMB is *not* sparse!

Exploiting sparsity
CMB contribution due to cosmic strings

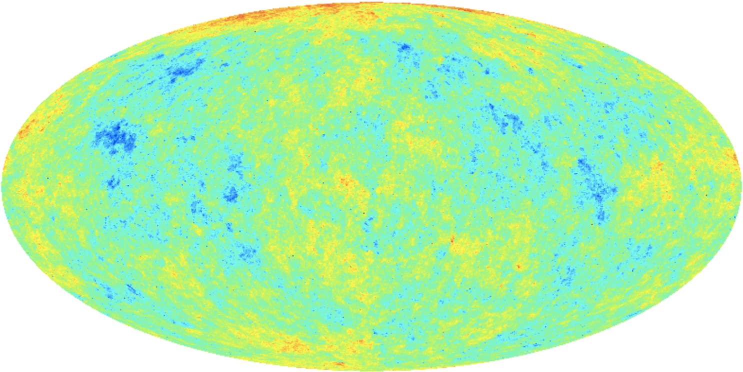

[Credit: Ringeval *et al.* (2012)]

Exploiting sparsity
Wavelet coefficients of CMB contribution due to cosmic strings

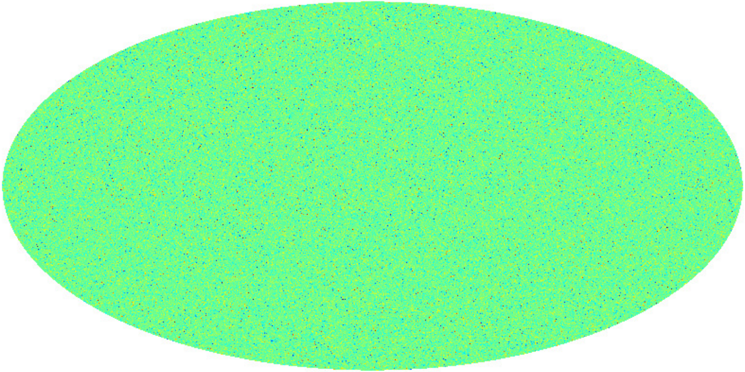

Other cosmological signals *are* sparse!

Exploiting sparsity
The correct approach

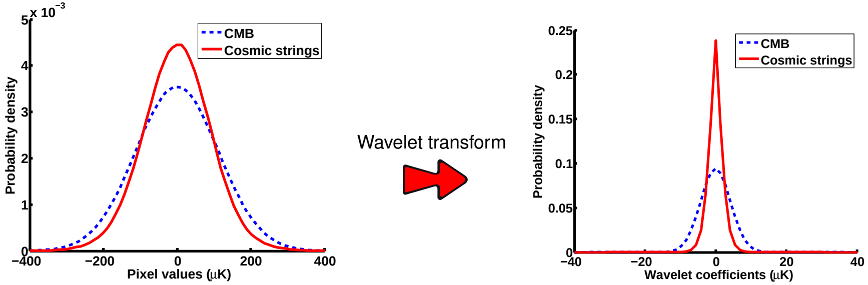

- While the CMB is not sparse, it may contain sparse contributions.
- Correct way to exploit sparsity is to treat, say, the CMB as (non-sparse) noise, and exploit sparsity of other cosmological or astrophysical signals.
- Not always the approach taken in the literature.

Exploiting sparsity
The correct approach

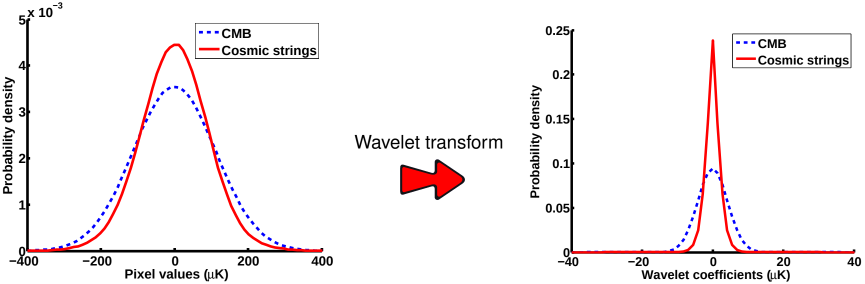

- While the CMB is not sparse, it may contain sparse contributions.
- Correct way to exploit sparsity is to treat, say, the CMB as (non-sparse) noise, and exploit sparsity of other cosmological or astrophysical signals.
- Not always the approach taken in the literature.

Cosmological observations live on spherical manifolds

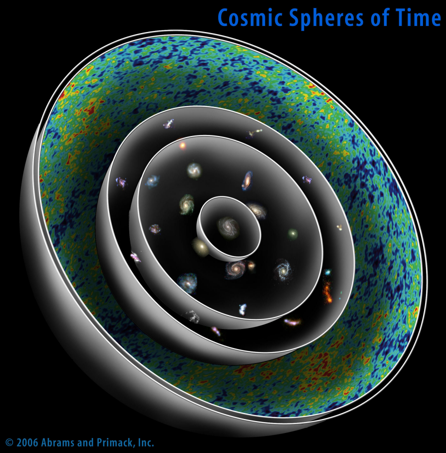

Outline

1. Harmonic analysis on the sphere
   - Sampling theorems
   - Wavelets
2. Harmonic analysis on the ball
   - Sampling theorems
   - Wavelets
3. Compressive Sensing
   - Synthesis-based
   - Analysis-based
   - Bayesian perspective
   - Sparsity averaging
   - Sphere
4. Cosmological applications
   - CMB inpainting
   - Cosmic strings

Outline

1. Harmonic analysis on the sphere
   - Sampling theorems
   - Wavelets
2. Harmonic analysis on the ball
   - Sampling theorems
   - Wavelets
3. Compressive Sensing
   - Synthesis-based
   - Analysis-based
   - Bayesian perspective
   - Sparsity averaging
   - Sphere
4. Cosmological applications
   - CMB inpainting
   - Cosmic strings

Cosmic microwave background (CMB)

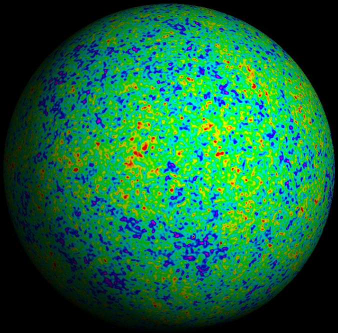

Credit: WMAP

Spherical harmonic transform

- The spherical harmonics are the eigenfunctions of the Laplacian on the sphere: $\Delta_{\mathbb{S}^2} Y_{\ell m} = -\ell(\ell+1) Y_{\ell m}$.

- A function on the sphere $f \in \mathrm{L}^2(\mathbb{S}^2)$ may be represented by its spherical harmonic expansion:

$$f(\theta, \varphi) = \sum_{\ell=0}^{\infty} \sum_{m=-\ell}^{\ell} f_{\ell m} \, Y_{\ell m}(\theta, \varphi) \ .$$

  where the spherical harmonic coefficients are given by:

$$f_{\ell m} = \langle f, \, Y_{\ell m} \rangle = \int_{\mathbb{S}^2} \mathrm{d}\Omega(\theta, \varphi) \, f(\theta, \varphi) \, Y_{\ell m}^*(\theta, \varphi) \ .$$

- Consider signals on the sphere band-limited at L, that is signals such that $f_{\ell m} = 0, \ \forall \ell \geq L$.

- For a band-limited signal, can we compute $f_{\ell m}$ exactly?

  → Sampling theorems on the sphere

Spherical harmonic transform

- The spherical harmonics are the eigenfunctions of the Laplacian on the sphere: $\Delta_{\mathbb{S}^2} Y_{\ell m} = -\ell(\ell+1) Y_{\ell m}$.

- A function on the sphere $f \in \mathrm{L}^2(\mathbb{S}^2)$ may be represented by its spherical harmonic expansion:

$$f(\theta, \varphi) = \sum_{\ell=0}^{\infty} \sum_{m=-\ell}^{\ell} f_{\ell m} \, Y_{\ell m}(\theta, \varphi) \ .$$

  where the spherical harmonic coefficients are given by:

$$f_{\ell m} = \langle f, \, Y_{\ell m} \rangle = \int_{\mathbb{S}^2} \mathrm{d}\Omega(\theta, \varphi) \, f(\theta, \varphi) \, Y_{\ell m}^*(\theta, \varphi) \ .$$

- Consider signals on the sphere band-limited at L, that is signals such that $\boxed{f_{\ell m} = 0, \ \forall \ell \geq L}$.

- For a band-limited signal, can we compute $f_{\ell m}$ exactly?

  $\rightarrow$ Sampling theorems on the sphere

Driscoll & Healy (DH) sampling theorem

- Canonical sampling theorem on the sphere derived by Driscoll & Healy (1994).

$\Rightarrow$ $N_{\rm DH} = (2L-1)2L + 1 \sim 4L^2$ samples on the sphere.

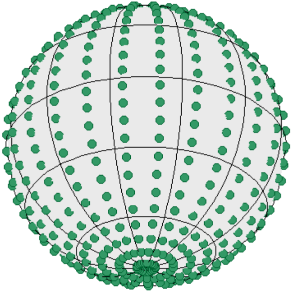

Figure: Sample positions of the DH sampling theorem.

McEwen & Wiaux (MW) sampling theorem

- A new sampling theorem on the sphere (McEwen & Wiaux 2011).

  $\Rightarrow$ $N_{\mathrm{MW}} = (L-1)(2L-1)+1 \sim 2L^2$ samples on the sphere.

- Reduced the Nyquist rate on the sphere by a factor of two.

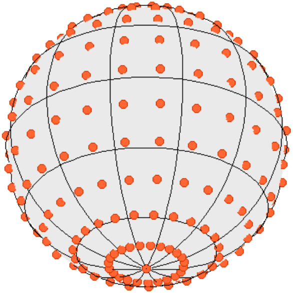

Figure: Sample positions of the MW sampling theorem.

McEwen & Wiaux (MW) sampling theorem

- New sampling theorem follows by associating the sphere with the torus through a periodic extension.
- Similar in flavour to making a periodic extension in θ of a function f on the sphere.

(a) Function on sphere (b) Even function on torus (c) Odd function on torus

Figure: Associating functions on the sphere and torus

Numerical accuracy

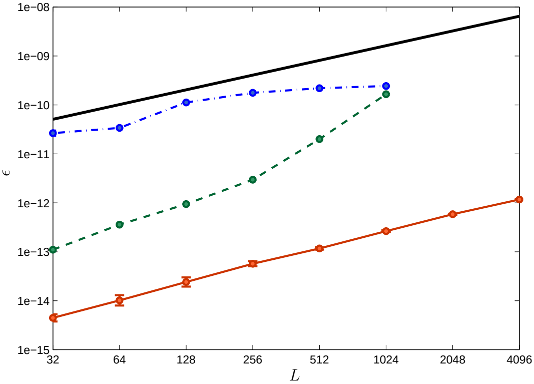

Figure: Numerical accuracy (MW=red; DH=green; GL=blue)

Computation time

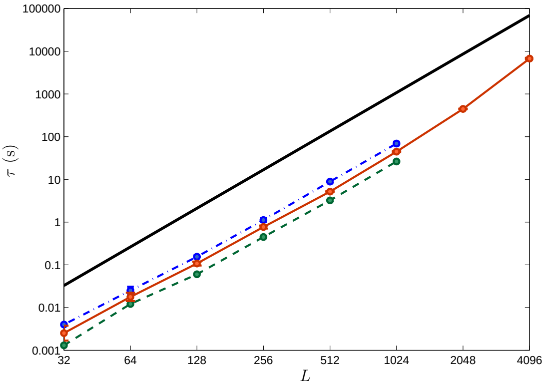

Figure: Computation time (MW=red; DH=green; GL=blue)

Code to compute (spin) spherical harmonic transforms

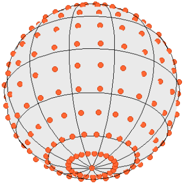

SSHT code: Spin spherical harmonic transforms
A novel sampling theorem on the sphere
McEwen & Wiaux (2011)

Code available from: `http://www.jasonmcewen.org/`

Wavelet transform in Euclidean space

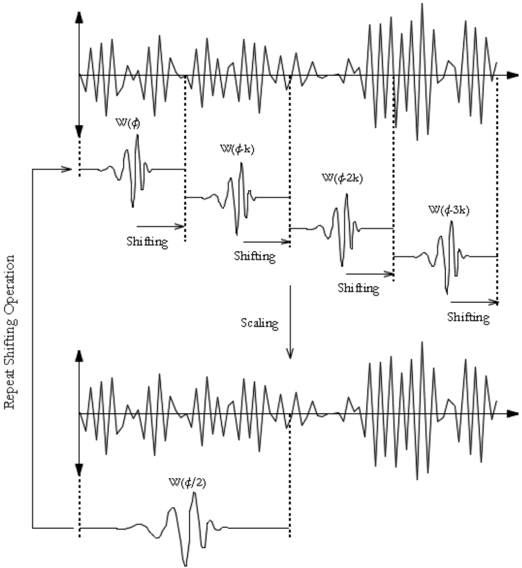

Figure: Wavelet scaling and shifting (Credit: http://www.wavelet.org/tutorial/)

Continuous wavelets on the sphere

- First natural wavelet construction on the sphere was derived in the seminal work of Antoine and Vandergheynst (1998) (reintroduced by Wiaux 2005).
- Construct wavelet atoms from affine transformations (dilation, translation) on the sphere of a mother wavelet.
- The natural extension of translations to the sphere are rotations. Rotation of a function f on the sphere is defined by

$$[\mathcal{R}(\rho)f](\omega) = f(\rho^{-1}\omega), \quad \omega = (\theta, \varphi) \in \mathbb{S}^2, \quad \rho = (\alpha, \beta, \gamma) \in \mathrm{SO}(3) \, .$$

- How define dilation on the sphere?
- The spherical dilation operator is defined through the conjugation of the Euclidean dilation and stereographic projection Π:

$$\mathcal{D}(a) \equiv \Pi^{-1} \, d(a) \, \Pi \, .$$

Continuous wavelets on the sphere

- First natural wavelet construction on the sphere was derived in the seminal work of Antoine and Vandergheynst (1998) (reintroduced by Wiaux 2005).
- Construct wavelet atoms from affine transformations (dilation, translation) on the sphere of a mother wavelet.
- The natural extension of translations to the sphere are rotations. Rotation of a function f on the sphere is defined by

$$[\mathcal{R}(\rho)f](\omega) = f(\rho^{-1}\omega), \quad \omega = (\theta, \varphi) \in \mathbb{S}^2, \quad \rho = (\alpha, \beta, \gamma) \in \mathrm{SO}(3) \; .$$

- How define dilation on the sphere?
- The spherical dilation operator is defined through the conjugation of the Euclidean dilation and stereographic projection Π:

$$\mathcal{D}(a) \equiv \Pi^{-1} \, d(a) \, \Pi \; .$$

Continuous wavelets on the sphere

- First natural wavelet construction on the sphere was derived in the seminal work of Antoine and Vandergheynst (1998) (reintroduced by Wiaux 2005).
- Construct wavelet atoms from affine transformations (dilation, translation) on the sphere of a mother wavelet.
- The natural extension of translations to the sphere are rotations. Rotation of a function f on the sphere is defined by

$$[\mathcal{R}(\rho)f](\omega) = f(\rho^{-1}\omega), \quad \omega = (\theta, \varphi) \in \mathbb{S}^2, \quad \rho = (\alpha, \beta, \gamma) \in \mathrm{SO}(3) \; .$$

- How define dilation on the sphere?
- The spherical dilation operator is defined through the conjugation of the Euclidean dilation and stereographic projection Π:

$$\mathcal{D}(a) \equiv \Pi^{-1}\, d(a)\, \Pi \; .$$

Continuous wavelets on the sphere

- First natural wavelet construction on the sphere was derived in the seminal work of Antoine and Vandergheynst (1998) (reintroduced by Wiaux 2005).
- Construct wavelet atoms from affine transformations (dilation, translation) on the sphere of a mother wavelet.
- The natural extension of translations to the sphere are rotations. Rotation of a function f on the sphere is defined by

$$[\mathcal{R}(\rho)f](\omega) = f(\rho^{-1}\omega), \quad \omega = (\theta, \varphi) \in \mathbb{S}^2, \quad \rho = (\alpha, \beta, \gamma) \in \mathrm{SO}(3) \ .$$

- How define dilation on the sphere?
- The spherical dilation operator is defined through the conjugation of the Euclidean dilation and stereographic projection Π:

$$\mathcal{D}(a) \equiv \Pi^{-1} \, d(a) \, \Pi \ .$$

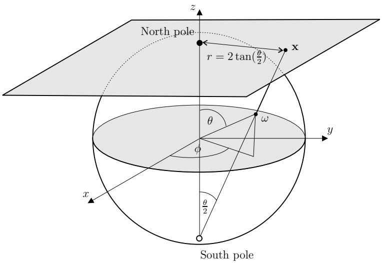

Figure: Stereographic projection.

Continuous wavelet analysis

- Wavelets on the sphere constructed from rotations and dilations of a mother spherical wavelet Ψ:

$$\{\Psi_{a,\rho} \equiv \mathcal{R}(\rho)\mathcal{D}(a)\Psi \,:\, \rho \in \mathrm{SO}(3),\, a \in \mathbb{R}_*^+\}.$$

- The forward wavelet transform is given by

$$W_\Psi^f(a,\rho) = \langle f, \Psi_{a,\rho}\rangle = \int_{\mathbb{S}^2} \mathrm{d}\Omega(\omega)\, f(\omega)\, \Psi_{a,\rho}^*(\omega) \,,$$

where $\mathrm{d}\Omega(\omega) = \sin\theta \,\mathrm{d}\theta \,\mathrm{d}\varphi$ is the usual invariant measure on the sphere.

- Transform general in the sense that all orientations in the rotation group $\mathrm{SO}(3)$ are considered, thus directional structure is naturally incorporated.

- Fast algorithms essential (for a review see Wiaux, McEwen & Vielva 2007)
  - Factoring of rotations: McEwen *et al.* (2007), Wandelt & Gorski (2001)
  - Separation of variables: Wiaux *et al.* (2005)

- FastCSWT code available to download: http://www.jasonmcewen.org/

Continuous wavelet analysis

- Wavelets on the sphere constructed from rotations and dilations of a mother spherical wavelet Ψ:

$$\{\Psi_{a,\rho} \equiv \mathcal{R}(\rho)\mathcal{D}(a)\Psi : \rho \in \mathrm{SO}(3),\, a \in \mathbb{R}^{+}_{*}\}.$$

- The forward wavelet transform is given by

$$W^{f}_{\Psi}(a,\rho) = \langle f, \Psi_{a,\rho} \rangle = \int_{\mathbb{S}^2} \mathrm{d}\Omega(\omega)\, f(\omega)\, \Psi^{*}_{a,\rho}(\omega)\ ,$$

  where $\mathrm{d}\Omega(\omega) = \sin\theta\, \mathrm{d}\theta\, \mathrm{d}\varphi$ is the usual invariant measure on the sphere.

- Transform general in the sense that all orientations in the rotation group $\mathrm{SO}(3)$ are considered, thus directional structure is naturally incorporated.

- Fast algorithms essential (for a review see Wiaux, McEwen & Vielva 2007)
  - Factoring of rotations: McEwen *et al.* (2007), Wandelt & Gorski (2001)
  - Separation of variables: Wiaux *et al.* (2005)

- FastCSWT code available to download: http://www.jasonmcewen.org/

Continuous wavelet analysis

- Wavelets on the sphere constructed from rotations and dilations of a mother spherical wavelet Ψ:

$$\{\Psi_{a,\rho} \equiv \mathcal{R}(\rho)\mathcal{D}(a)\Psi : \rho \in \mathrm{SO}(3),\, a \in \mathbb{R}^{+}_{*}\}.$$

- The forward wavelet transform is given by

$$\boxed{W^{f}_{\Psi}(a, \rho) = \langle f, \Psi_{a,\rho} \rangle = \int_{\mathbb{S}^2} \mathrm{d}\Omega(\omega)\, f(\omega)\, \Psi^{*}_{a,\rho}(\omega)\ ,}$$

  where $\mathrm{d}\Omega(\omega) = \sin\theta\, \mathrm{d}\theta\, \mathrm{d}\varphi$ is the usual invariant measure on the sphere.

- Transform general in the sense that all orientations in the rotation group $\mathrm{SO}(3)$ are considered, thus directional structure is naturally incorporated.

- Fast algorithms essential (for a review see Wiaux, McEwen & Vielva 2007)
  - Factoring of rotations: McEwen *et al.* (2007), Wandelt & Gorski (2001)
  - Separation of variables: Wiaux *et al.* (2005)

- FastCSWT code available to download: `http://www.jasonmcewen.org/`

Continuous wavelet synthesis (reconstruction)

- The inverse wavelet transform given by

$$f(\omega) = \int_0^\infty \frac{\mathrm{d}a}{a^3} \int_{\mathrm{SO}(3)} \mathrm{d}\varrho(\rho) W_\Psi^f(a,\rho) \, [\mathcal{R}(\rho) \widehat{L}_\Psi \Psi_a](\omega) \; ,$$

where $\mathrm{d}\varrho(\rho) = \sin\beta \, \mathrm{d}\alpha \, \mathrm{d}\beta \, \mathrm{d}\gamma$ is the invariant measure on the rotation group $\mathrm{SO}(3)$.

- Perfect reconstruction is ensured provided wavelets satisfy the admissibility property:

$$0 < \widehat{C}_\Psi^\ell \equiv \frac{8\pi^2}{2\ell+1} \sum_{m=-\ell}^{\ell} \int_0^\infty \frac{\mathrm{d}a}{a^3} \mid (\Psi_a)_{\ell m} \mid^2 < \infty, \quad \forall \ell \in \mathbb{N}$$

where $(\Psi_a)_{\ell m}$ are the spherical harmonic coefficients of $\Psi_a(\omega)$.

- Continuous wavelets used effectively in many cosmological studies, for example:
  - Non-Gaussianity (*e.g.* Vielva *et al.* 2004; McEwen *et al.* 2005, 2006, 2008)
  - ISW (*e.g.* Vielva *et al.* 2005, McEwen *et al.* 2007, 2008)

- BUT...

Continuous wavelet synthesis (reconstruction)

- The inverse wavelet transform given by

$$f(\omega) = \int_0^\infty \frac{\mathrm{d}a}{a^3} \int_{\mathrm{SO}(3)} \mathrm{d}\varrho(\rho) W^f_\Psi(a,\rho) \, [\mathcal{R}(\rho)\widehat{L}_\Psi \Psi_a](\omega) \; ,$$

where $\mathrm{d}\varrho(\rho) = \sin\beta \, \mathrm{d}\alpha \, \mathrm{d}\beta \, \mathrm{d}\gamma$ is the invariant measure on the rotation group $\mathrm{SO}(3)$.

- Perfect reconstruction is ensured provided wavelets satisfy the admissibility property:

$$0 < \widehat{C}^\ell_\Psi \equiv \frac{8\pi^2}{2\ell+1} \sum_{m=-\ell}^{\ell} \int_0^\infty \frac{\mathrm{d}a}{a^3} \mid (\Psi_a)_{\ell m} \mid^2 < \infty, \quad \forall \ell \in \mathbb{N}$$

where $(\Psi_a)_{\ell m}$ are the spherical harmonic coefficients of $\Psi_a(\omega)$.

- Continuous wavelets used effectively in many cosmological studies, for example:
  - Non-Gaussianity (*e.g.* Vielva *et al.* 2004; McEwen *et al.* 2005, 2006, 2008)
  - ISW (*e.g.* Vielva *et al.* 2005, McEwen *et al.* 2007, 2008)

- BUT...

Continuous wavelet synthesis (reconstruction)

- The inverse wavelet transform given by

$$f(\omega) = \int_0^\infty \frac{\mathrm{d}a}{a^3} \int_{\mathrm{SO}(3)} \mathrm{d}\varrho(\rho) W_\Psi^f(a,\rho) \, [\mathcal{R}(\rho)\widehat{L}_\Psi \Psi_a](\omega) \; ,$$

where $\mathrm{d}\varrho(\rho) = \sin\beta \, \mathrm{d}\alpha \, \mathrm{d}\beta \, \mathrm{d}\gamma$ is the invariant measure on the rotation group $\mathrm{SO}(3)$.

- Perfect reconstruction is ensured provided wavelets satisfy the admissibility property:

$$0 < \widehat{C}_\Psi^\ell \equiv \frac{8\pi^2}{2\ell+1} \sum_{m=-\ell}^{\ell} \int_0^\infty \frac{\mathrm{d}a}{a^3} \mid (\Psi_a)_{\ell m} \mid^2 < \infty, \quad \forall \ell \in \mathbb{N}$$

where $(\Psi_a)_{\ell m}$ are the spherical harmonic coefficients of $\Psi_a(\omega)$.

- Continuous wavelets used effectively in many cosmological studies, for example:
  - Non-Gaussianity (*e.g.* Vielva *et al.* 2004; McEwen *et al.* 2005, 2006, 2008)
  - ISW (*e.g.* Vielva *et al.* 2005, McEwen *et al.* 2007, 2008)

- BUT... **exact reconstruction not feasible in practice!**

Scale-discretised wavelets on the sphere

- **Exact reconstruction not feasible in practice with continuous wavelets!**

- Wiaux, McEwen, Vandergheynst, Blanc (2008)
  Exact reconstruction with directional wavelets on the sphere
  S2DW code

- Dilation performed in harmonic space.
  Following McEwen *et al.* (2006), Sanz *et al.* (2006).

- The scale-discretised wavelet $\Psi \in \mathrm{L}^2(\mathrm{S}^2, \mathrm{d}\Omega)$ is defined in harmonic space:

$$\widehat{\Psi}_{\ell m} = \tilde{K}_\Psi(\ell) S^\Psi_{\ell m} \, .$$

- Construct wavelets to satisfy a resolution of the identity for $0 \leq \ell < L$:

$$\tilde{\Phi}^2_\Psi(\alpha^J \ell) + \sum_{j=0}^{J} \tilde{K}^2_\Psi(\alpha^j \ell) = 1 \, .$$

Scale-discretised wavelets on the sphere

- **Exact reconstruction not feasible in practice with continuous wavelets!**
- Wiaux, McEwen, Vandergheynst, Blanc (2008)
  Exact reconstruction with directional wavelets on the sphere
  S2DW code

- Dilation performed in harmonic space.
  Following McEwen *et al.* (2006), Sanz *et al.* (2006).
- The scale-discretised wavelet $\Psi \in \mathrm{L}^2(\mathrm{S}^2, \mathrm{d}\Omega)$ is defined in harmonic space:

$$\widehat{\Psi}_{\ell m} = \tilde{K}_{\Psi}(\ell) S^{\Psi}_{\ell m} \, .$$

- Construct wavelets to satisfy a resolution of the identity for $0 \leq \ell < L$:

$$\tilde{\Phi}^2_{\Psi}(\alpha^J \ell) + \sum_{j=0}^{J} \tilde{K}^2_{\Psi}(\alpha^j \ell) = 1 \, .$$

Scale-discretised wavelets on the sphere

- **Exact reconstruction not feasible in practice with continuous wavelets!**
- Wiaux, McEwen, Vandergheynst, Blanc (2008)
  Exact reconstruction with directional wavelets on the sphere
  S2DW code

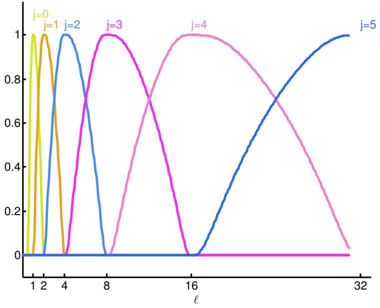

Figure: Harmonic tiling on the sphere.

- Dilation performed in harmonic space.
  Following McEwen *et al.* (2006), Sanz *et al.* (2006).
- The scale-discretised wavelet $\Psi \in \mathrm{L}^2(\mathrm{S}^2, \mathrm{d}\Omega)$ is defined in harmonic space:

$$\widehat{\Psi}_{\ell m} = \tilde{K}_\Psi(\ell) S^{\Psi}_{\ell m} \ .$$

- Construct wavelets to satisfy a resolution of the identity for $0 \leq \ell < L$:

$$\tilde{\Phi}^2_\Psi(\alpha^J \ell) + \sum_{j=0}^{J} \tilde{K}^2_\Psi(\alpha^j \ell) = 1 \ .$$

Scale-discretised wavelets on the sphere

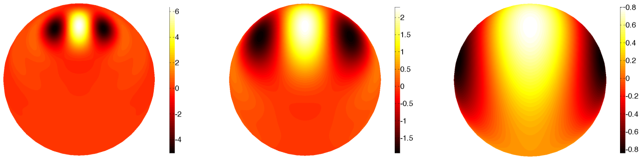

Figure: Spherical scale-discretised wavelets.

- Construct directional and steerable wavelets.

- The scale-discretised wavelet transform is given by the usual projection onto each wavelet:

$$W^f_\Psi(\rho, \alpha^j) = \langle f, \Psi_{\rho,\alpha^j} \rangle = \int_{\mathbb{S}^2} \mathrm{d}\Omega(\omega)\, f(\omega)\, \Psi^*_{\rho,\alpha^j}(\omega) .$$

- The original function may be recovered exactly in practice from the wavelet (and scaling) coefficients:

$$f(\omega) = [\Phi_{\alpha^J} f](\omega) + \sum_{j=0}^{J} \int_{\mathrm{SO}(3)} \mathrm{d}\varrho(\rho)\, W^f_\Psi\left(\rho, \alpha^j\right) \left[R(\rho)\, L^{\mathrm{d}} \Psi_{\alpha^j}\right](\omega) .$$

Scale-discretised wavelets on the sphere

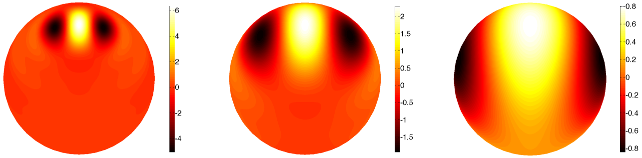

Figure: Spherical scale-discretised wavelets.

- Construct directional and steerable wavelets.
- The scale-discretised wavelet transform is given by the usual projection onto each wavelet:

$$W^f_{\Psi}(\rho, \alpha^j) = \langle f, \Psi_{\rho,\alpha^j} \rangle = \int_{\mathbb{S}^2} \mathrm{d}\Omega(\omega)\, f(\omega)\, \Psi^*_{\rho,\alpha^j}(\omega) \,.$$

- The original function may be recovered exactly in practice from the wavelet (and scaling) coefficients:

$$f(\omega) = [\Phi_{\alpha^J} f](\omega) + \sum_{j=0}^{J} \int_{\mathrm{SO}(3)} \mathrm{d}\varrho(\rho)\, W^f_{\Psi}\left(\rho, \alpha^j\right) \left[R(\rho)\, L^{\mathrm{d}} \Psi_{\alpha^j}\right](\omega) \,.$$

Scale-discretised wavelets on the sphere

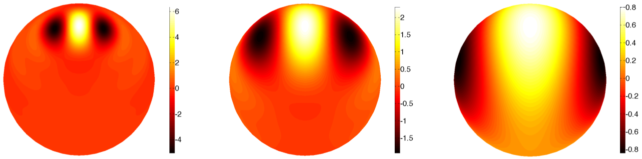

Figure: Spherical scale-discretised wavelets.

- Construct directional and steerable wavelets.
- The scale-discretised wavelet transform is given by the usual projection onto each wavelet:

$$W^f_{\Psi}(\rho, \alpha^j) = \langle f, \Psi_{\rho,\alpha^j} \rangle = \int_{\mathbb{S}^2} \mathrm{d}\Omega(\omega)\, f(\omega)\, \Psi^*_{\rho,\alpha^j}(\omega) \, .$$

- The original function may be recovered exactly in practice from the wavelet (and scaling) coefficients:

$$f(\omega) = \left[\Phi_{\alpha^J} f\right](\omega) + \sum_{j=0}^{J} \int_{\mathrm{SO}(3)} \mathrm{d}\varrho(\rho)\, W^f_{\Psi}\left(\rho, \alpha^j\right) \left[R(\rho)\, L^{\mathrm{d}} \Psi_{\alpha^j}\right](\omega) \, .$$

Scale-discretised wavelet transform of the Earth

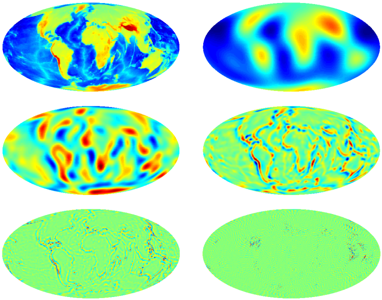

(a) Undecimated

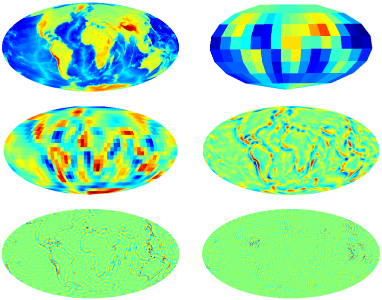

(b) Multi-resolution

Figure: Scale-discretised wavelet transform of a topography map of the Earth.

Codes to compute scale-discretised wavelets on the sphere

S2DW code

Exact reconstruction with directional wavelets on the sphere

Wiaux, McEwen, Vandergheynst, Blanc (2008)

- Fortran
- Parallelised
- Supports directional, steerable wavelets

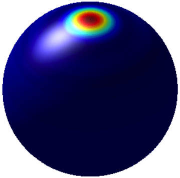

S2LET code

S2LET: A code to perform fast wavelet analysis on the sphere

Leistedt, McEwen, Vandergheynst, Wiaux (2012)

- C, Matlab, IDL, Java
- Support only axisymmetric wavelets at present
- Future extensions:
  - Directional, steerable wavelets
  - Faster algorithms to perform wavelet transforms
  - Spin wavelets

All codes available from: `http://www.jasonmcewen.org/`

Outline

Galaxy surveys

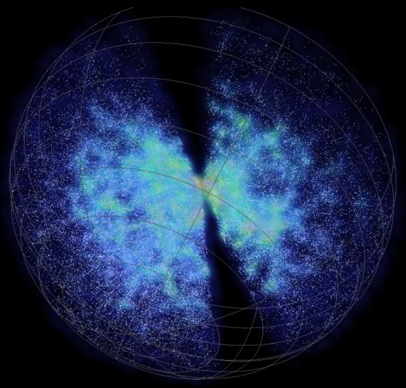

Credit: SDSS

Sampling theorem on the ball

- Fourier-Bessel functions are the canonical orthogonal basis on the sphere $\rightarrow$ but do not admit a sampling theorem.
- Developed a new Fourier-Laguerre transform and the first sampling theorem on the ball (Leistedt & McEwen 2012).
- Define the radial basis functions by

$$K_p(r) \equiv \sqrt{\frac{p!}{(p+2)!}} \frac{e^{-r/2\tau}}{\sqrt{\tau^3}} L_p^{(2)}\left(\frac{r}{\tau}\right),$$

where $L_p^{(2)}$ is the p-th generalised Laguerre polynomial of order two.

- Define the Fourier-Laguerre basis functions by $Z_{\ell mp}(\boldsymbol{r}) = K_p(r) Y_{\ell m}(\omega)$.

Sampling theorem on the ball

- Fourier-Bessel functions are the canonical orthogonal basis on the sphere → but do not admit a sampling theorem.
- Developed a new Fourier-Laguerre transform and the first sampling theorem on the ball (Leistedt & McEwen 2012).
- Define the radial basis functions by

$$K_p(r) \equiv \sqrt{\frac{p!}{(p+2)!}} \frac{e^{-r/2\tau}}{\sqrt{\tau^3}} L_p^{(2)}\left(\frac{r}{\tau}\right) ,$$

  where $L_p^{(2)}$ is the p-th generalised Laguerre polynomial of order two.
- Define the Fourier-Laguerre basis functions by $Z_{\ell mp}(\mathbf{r}) = K_p(r) Y_{\ell m}(\omega)$.

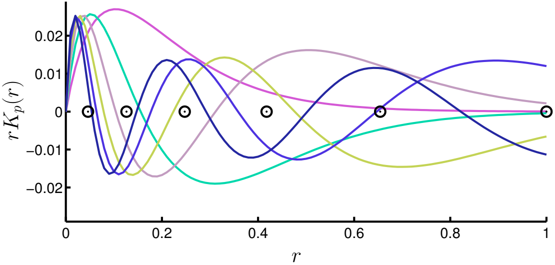

Figure: Functions $rK_p(r)$]

Sampling theorem on the ball

- For a band-limited signal, we can compute the Fourier-Laguerre transform exactly.
- Compute Fourier-Bessel coefficients exactly from Fourier-Laguerre coefficients.

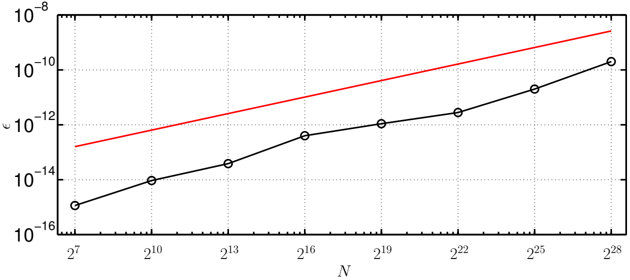

Figure: Numerical accuracy of Fourier-Laguerre transform

Sampling theorem on the ball

- Fast algorithms to compute the Fourier-Laguerre transform.

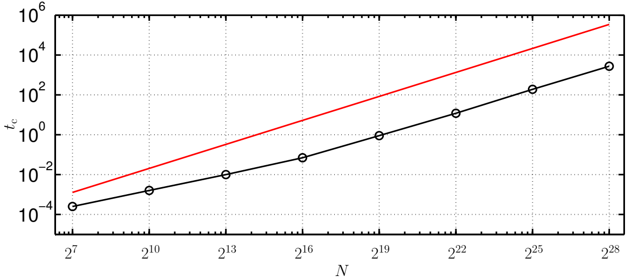

Figure: Computation time of Fourier-Laguerre transform

Code to compute the Fourier-Laguerre transform

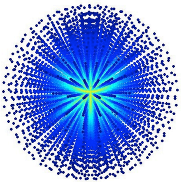

FLAG code: Fourier-Laguerre transforms

Exact wavelets on the ball

Leistedt & McEwen (2012)

All codes available from: `http://www.jasonmcewen.org/`

Translation and convolution on the radial line

- We construct translation and convolution operators on the radial line by analogy with the infinite line.
- For the standard orthogonal basis $\phi_\omega(x) = e^{i\omega x}$ translation of the basis functions defined by the shift of coordinates:

$$(\mathcal{T}_u^{\mathbb{R}} \phi_\omega)(x) \equiv \phi_\omega(x-u) = \phi_\omega^*(u)\phi_\omega(x) \ .$$

- Define translation of the spherical Laguerre basis functions on the radial line by analogy:

$$(\mathcal{T}_s K_p)(r) \equiv K_p(s) K_p(r) \ .$$

- Define convolution on the radial line of by

$$(f \star h)(r) \equiv \langle f | \mathcal{T}_r h \rangle = \int_{\mathbb{R}+} ds s^2 f(s) \, (\mathcal{T}_r h)\,(s),$$

from which it follows that radial convolution in harmonic space is given by the product

$$(f \star h)_p = \langle f \star h | K_p \rangle = f_p h_p \ .$$

Translation and convolution on the radial line

- We construct translation and convolution operators on the radial line by analogy with the infinite line.

- For the standard orthogonal basis $\phi_\omega(x) = e^{i\omega x}$ translation of the basis functions defined by the shift of coordinates:

$$(\mathcal{T}_u^{\mathbb{R}} \phi_\omega)(x) \equiv \phi_\omega(x-u) = \phi_\omega^*(u)\phi_\omega(x) \ .$$

- Define translation of the spherical Laguerre basis functions on the radial line by analogy:

$$(\mathcal{T}_s K_p)(r) \equiv K_p(s) K_p(r) \ .$$

- Define convolution on the radial line of by

$$(f \star h)(r) \equiv \langle f | \mathcal{T}_r h \rangle = \int_{\mathbb{R}+} \mathrm{d}s s^2 f(s) \left(\mathcal{T}_r h\right)(s),$$

from which it follows that radial convolution in harmonic space is given by the product

$$(f \star h)_p = \langle f \star h | K_p \rangle = f_p h_p \ .$$

Translation and convolution on the radial line

- We construct translation and convolution operators on the radial line by analogy with the infinite line.

- For the standard orthogonal basis $\phi_\omega(x) = e^{i\omega x}$ translation of the basis functions defined by the shift of coordinates:

$$(\mathcal{T}_u^{\mathbb{R}} \phi_\omega)(x) \equiv \phi_\omega(x-u) = \phi_\omega^*(u)\phi_\omega(x) \; .$$

- Define translation of the spherical Laguerre basis functions on the radial line by analogy:

$$(\mathcal{T}_s K_p)(r) \equiv K_p(s) K_p(r) \; .$$

- Define convolution on the radial line of by

$$(f \star h)(r) \equiv \langle f | \mathcal{T}_r h \rangle = \int_{\mathbb{R}+} \mathrm{d}s s^2 f(s) \left(\mathcal{T}_r h\right)(s),$$

from which it follows that radial convolution in harmonic space is given by the product

$$(f \star h)_p = \langle f \star h | K_p \rangle = f_p h_p \; .$$

Translation and convolution on the radial line

- Translation corresponds to convolution with the Dirac delta:

$$(f \star \delta_s)(r) = \sum_{p=0}^{\infty} f_p K_p(s) K_p(r) = (\mathcal{T}_s f)(r) \ .$$

- Angular aperture of localised functions (and flaglets) is invariant under radial translation.

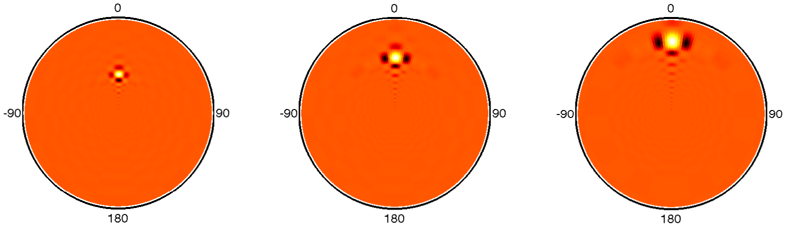

(a) Translated by $r = 0.2$ (b) Translated by $r = 0.3$ (c) Translated by $r = 0.4$

Figure: Slices of an axisymmetric flaglet wavelet plotted on the ball of radius $R = 0.5$.

Scale-discretised wavelets on the ball

- *Exact wavelets on the ball* (Leistedt & McEwen 2012).
- Define translation and convolution operators on the radial line.
- Dilation performed in harmonic space.
- Scale-discretised wavelet $\Psi \in \mathrm{L}^2(B^3)$ is defined in harmonic space:

$$\Psi^{jj'}_{\ell mp} \equiv \sqrt{\frac{2\ell+1}{4\pi}}\, \kappa_\lambda\!\left(\frac{\ell}{\lambda^j}\right) \kappa_\nu\!\left(\frac{p}{\nu^{j'}}\right) \delta_{m0}\,.$$

- Construct wavelets to satisfy a resolution of the identity:

$$\frac{4\pi}{2\ell+1}\left(|\Phi_{\ell 0 p}|^2 + \sum_{j=J_0}^{J} \sum_{j'=J'_0}^{J'} |\Psi^{jj'}_{\ell 0 p}|^2 \right) = 1, \ \forall \ell, p\,.$$

Scale-discretised wavelets on the ball

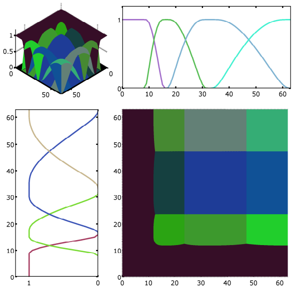

Figure: Tiling of Fourier-Laguerre space.

- *Exact wavelets on the ball* (Leistedt & McEwen 2012).
- Define translation and convolution operators on the radial line.
- Dilation performed in harmonic space.
- Scale-discretised wavelet $\Psi \in \mathrm{L}^2(B^3)$ is defined in harmonic space:

$$\Psi^{jj'}_{\ell mp} \equiv \sqrt{\frac{2\ell+1}{4\pi}}\,\kappa_\lambda\left(\frac{\ell}{\lambda^j}\right)\kappa_\nu\left(\frac{p}{\nu^{j'}}\right)\delta_{m0}\,.$$

- Construct wavelets to satisfy a resolution of the identity:

$$\frac{4\pi}{2\ell+1}\left(|\Phi_{\ell 0p}|^2 + \sum_{j=J_0}^{J}\sum_{j'=J'_0}^{J'}|\Psi^{jj'}_{\ell 0p}|^2\right) = 1,\ \forall \ell, p.$$

Scale-discretised wavelets on the ball

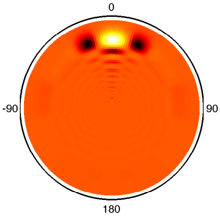

(a) $(j, j') = (4, 5)$

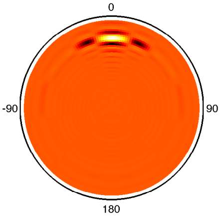

(b) $(j, j') = (4, 6)$

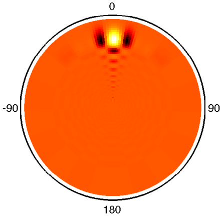

(c) $(j, j') = (5, 5)$

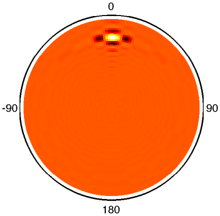

(d) $(j, j') = (5, 6)$

Figure: Scale-discretised wavelets on the ball.

Scale-discretised wavelets on the ball

- The scale-discretised wavelet transform is given by the usual projection onto each wavelet:

$$W^{\Psi^{jj'}}(\boldsymbol{r}) \equiv (f \star \Psi^{jj'})(\boldsymbol{r}) = \langle f | \mathcal{T}_r \mathcal{R}_\omega \Psi^{jj'} \rangle \ .$$

- The original function may be recovered exactly in practice from the wavelet (and scaling) coefficients:

$$f(\boldsymbol{r}) \quad = \quad \int_{B^3} \mathrm{d}^3\boldsymbol{r}' \, W^{\Phi}(\boldsymbol{r}')(\mathcal{T}_r \mathcal{R}_\omega \Phi)(\boldsymbol{r}') + \sum_{j=J_0}^{J} \sum_{j'=J'_0}^{J'} \int_{B^3} \mathrm{d}^3\boldsymbol{r}' \, W^{\Psi^{jj'}}(\boldsymbol{r}')(\mathcal{T}_r \mathcal{R}_\omega \Psi^{jj'})(\boldsymbol{r}') \ .$$

Scale-discretised wavelet denoising on the ball

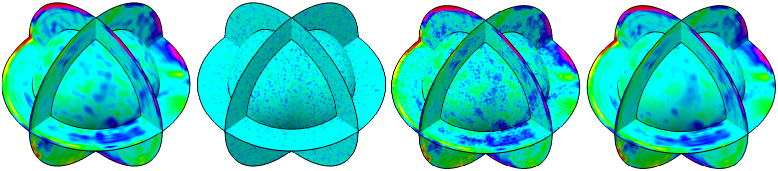

(a) Ground truth (b) Noise (c) Noisy (SNR=5dB) (d) Denoised (SNR=17dB)

Figure: Denoising of a seismological Earth model.

Scale-discretised wavelet denoising on the ball

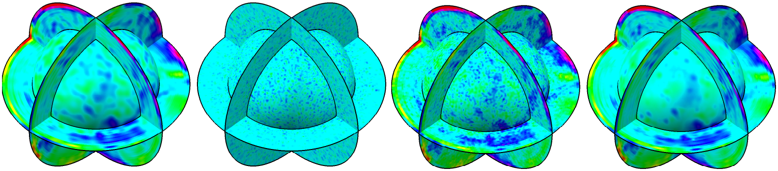

(a) Ground truth (b) Noise (c) Noisy (SNR=5dB) (d) Denoised (SNR=17dB)

Figure: Denoising of a seismological Earth model.

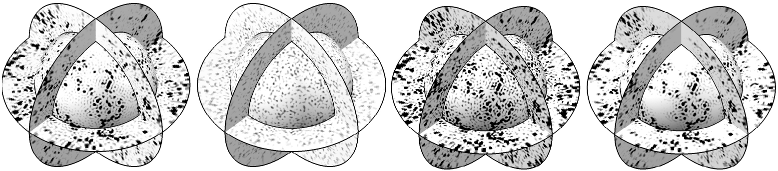

(a) Ground truth (b) Noise (c) Noisy (SNR=5dB) (d) Denoised (SNR=11dB)

Figure: Denoising of an N-body simulation.

Code for scale-discretised wavelets on the ball

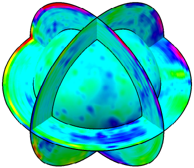

FLAGLET code
Exact wavelets on the ball
Leistedt & McEwen (2012)

- C, Matlab, IDL, Java
- Exact (Fourier-LAGuerre) wavelets on the ball – coined *flaglets*!

Code available from: `http://www.jasonmcewen.org/`

Outline

1. Harmonic analysis on the sphere
   - Sampling theorems
   - Wavelets
2. Harmonic analysis on the ball
   - Sampling theorems
   - Wavelets
3. Compressive Sensing
   - Synthesis-based
   - Analysis-based
   - Bayesian perspective
   - Sparsity averaging
   - Sphere
4. Cosmological applications
   - CMB inpainting
   - Cosmic strings

Compressive sensing

- Next evolution of wavelet analysis $\rightarrow$ wavelets are a key ingredient.
- The mystery of JPEG compression (discrete cosine transform; wavelet transform).
- Move compression to the acquisition stage $\rightarrow$ compressive sensing.
- Acquisition versus imaging.

Compressive sensing

- Next evolution of wavelet analysis $\rightarrow$ wavelets are a key ingredient.
- The mystery of JPEG compression (discrete cosine transform; wavelet transform).
- Move compression to the acquisition stage $\rightarrow$ compressive sensing.
- Acquisition versus imaging.

Compressive sensing

- Next evolution of wavelet analysis → wavelets are a key ingredient.
- The mystery of JPEG compression (discrete cosine transform; wavelet transform).
- Move compression to the acquisition stage → compressive sensing.
- Acquisition versus imaging.

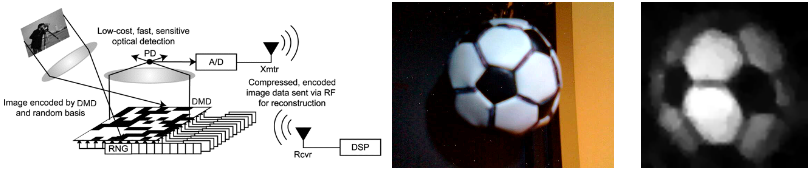

(a) Architecture (b) Scene (c) Recov. (20% meas.)

Figure: Single pixel camera

Compressive sensing

- Next evolution of wavelet analysis $\rightarrow$ wavelets are a key ingredient.
- The mystery of JPEG compression (discrete cosine transform; wavelet transform).
- Move compression to the acquisition stage $\rightarrow$ compressive sensing.
- Acquisition versus imaging.

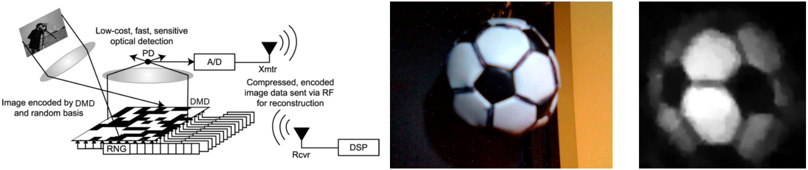

(a) Architecture (b) Scene (c) Recov. (20% meas.)

Figure: Single pixel camera

An introduction to compressive sensing

- Linear operator (algebra) representation of signal decomposition (into *atoms* of a *dictionary*):

$$x(t) = \sum_i \alpha_i \Psi_i(t) \quad \rightarrow \quad \boldsymbol{x} = \sum_i \Psi_i \alpha_i = \begin{pmatrix} | \\ \Psi_0 \\ | \end{pmatrix} \alpha_0 + \begin{pmatrix} | \\ \Psi_1 \\ | \end{pmatrix} \alpha_1 + \cdots \quad \rightarrow \quad \boxed{\boldsymbol{x} = \Psi \boldsymbol{\alpha}}$$

- Linear operator (algebra) representation of measurement:

$$y_i = \langle x, \Phi_j \rangle \quad \rightarrow \quad \boldsymbol{y} = \begin{pmatrix} - \ \Phi_0 \ - \\ - \ \Phi_1 \ - \\ \vdots \end{pmatrix} \boldsymbol{x} \quad \rightarrow \quad \boxed{\boldsymbol{y} = \Phi \boldsymbol{x}}$$

- Putting it together: $\boxed{\boldsymbol{y} = \Phi \boldsymbol{x} = \Phi \Psi \boldsymbol{\alpha}}$

An introduction to compressive sensing

- Linear operator (algebra) representation of signal decomposition (into *atoms* of a *dictionary*):

$$x(t) = \sum_i \alpha_i \Psi_i(t) \quad \rightarrow \quad \boldsymbol{x} = \sum_i \Psi_i \alpha_i = \begin{pmatrix} | \\ \Psi_0 \\ | \end{pmatrix} \alpha_0 + \begin{pmatrix} | \\ \Psi_1 \\ | \end{pmatrix} \alpha_1 + \cdots \quad \rightarrow \quad \boxed{\boldsymbol{x} = \Psi \boldsymbol{\alpha}}$$

- Linear operator (algebra) representation of measurement:

$$y_i = \langle x, \Phi_j \rangle \quad \rightarrow \quad \boldsymbol{y} = \begin{pmatrix} - \ \Phi_0 \ - \\ - \ \Phi_1 \ - \\ \vdots \end{pmatrix} \boldsymbol{x} \quad \rightarrow \quad \boxed{\boldsymbol{y} = \Phi \boldsymbol{x}}$$

- Putting it together: $\boxed{\boldsymbol{y} = \Phi \boldsymbol{x} = \Phi \Psi \boldsymbol{\alpha}}$

An introduction to compressive sensing

- Linear operator (algebra) representation of signal decomposition (into *atoms* of a *dictionary*):

$$x(t) = \sum_i \alpha_i \Psi_i(t) \quad \rightarrow \quad \boldsymbol{x} = \sum_i \Psi_i \alpha_i = \begin{pmatrix} | \\ \Psi_0 \\ | \end{pmatrix} \alpha_0 + \begin{pmatrix} | \\ \Psi_1 \\ | \end{pmatrix} \alpha_1 + \cdots \quad \rightarrow \quad \boxed{\boldsymbol{x} = \Psi \boldsymbol{\alpha}}$$

- Linear operator (algebra) representation of measurement:

$$y_i = \langle x, \Phi_j \rangle \quad \rightarrow \quad \boldsymbol{y} = \begin{pmatrix} - & \Phi_0 & - \\ - & \Phi_1 & - \\ & \vdots & \end{pmatrix} \boldsymbol{x} \quad \rightarrow \quad \boxed{\boldsymbol{y} = \Phi \boldsymbol{x}}$$

- Putting it together: $\boxed{\boldsymbol{y} = \Phi \boldsymbol{x} = \Phi \Psi \boldsymbol{\alpha}}$

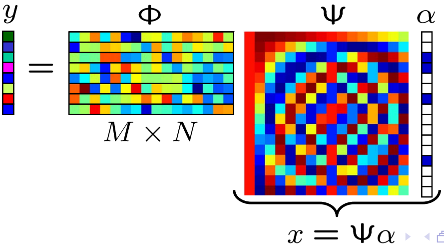

An introduction to compressive sensing

- Ill-posed inverse problem:

$$\boldsymbol{y} = \Phi \boldsymbol{x} + \boldsymbol{n} = \Phi \Psi \boldsymbol{\alpha} + \boldsymbol{n} .$$

- Solve by imposing a regularising prior that the signal to be recovered is sparse in Ψ, *i.e.* solve the following ℓ_0 optimisation problem:

$$\boldsymbol{\alpha}^\star = \arg\min_{\boldsymbol{\alpha}} \|\alpha\|_0 \text{ such that } \|\boldsymbol{y} - \Phi\Psi\boldsymbol{\alpha}\|_2 \leq \epsilon ,$$

  where the signal is synthesising by $\boldsymbol{x}^\star = \Psi \boldsymbol{\alpha}^\star$.

- Recall norms given by:

$$\|\alpha\|_0 = \text{no. non-zero elements} \qquad \|\alpha\|_1 = \sum_i |\alpha_i| \qquad \|\alpha\|_2 = \Big(\sum_i |\alpha_i|^2\Big)^{1/2}$$

- Solving this problem is difficult (combinatorial).

- Instead, solve the ℓ_1 optimisation problem (convex):

$$\boldsymbol{\alpha}^\star = \arg\min_{\boldsymbol{\alpha}} \|\alpha\|_1 \text{ such that } \|\boldsymbol{y} - \Phi\Psi\boldsymbol{\alpha}\|_2 \leq \epsilon .$$

An introduction to compressive sensing

- Ill-posed inverse problem:

$$\boldsymbol{y} = \Phi \boldsymbol{x} + \boldsymbol{n} = \Phi \Psi \boldsymbol{\alpha} + \boldsymbol{n} .$$

- Solve by imposing a regularising prior that the signal to be recovered is sparse in Ψ, *i.e.* solve the following ℓ_0 optimisation problem:

$$\boldsymbol{\alpha}^\star = \underset{\boldsymbol{\alpha}}{\arg\min} \|\alpha\|_0 \text{ such that } \|\boldsymbol{y} - \Phi\Psi\boldsymbol{\alpha}\|_2 \leq \epsilon ,$$

  where the signal is synthesising by $\boldsymbol{x}^\star = \Psi \boldsymbol{\alpha}^\star$.

- Recall norms given by:

$$\|\alpha\|_0 = \text{no. non-zero elements} \qquad \|\alpha\|_1 = \sum_i |\alpha_i| \qquad \|\alpha\|_2 = \Big(\sum_i |\alpha_i|^2\Big)^{1/2}$$

- Solving this problem is difficult (combinatorial).

- Instead, solve the ℓ_1 optimisation problem (convex):

$$\boldsymbol{\alpha}^\star = \underset{\boldsymbol{\alpha}}{\arg\min} \|\alpha\|_1 \text{ such that } \|\boldsymbol{y} - \Phi\Psi\boldsymbol{\alpha}\|_2 \leq \epsilon .$$

An introduction to compressive sensing

- Ill-posed inverse problem:

$$\boldsymbol{y} = \Phi \boldsymbol{x} + \boldsymbol{n} = \Phi \Psi \boldsymbol{\alpha} + \boldsymbol{n} .$$

- Solve by imposing a regularising prior that the signal to be recovered is sparse in Ψ, *i.e.* solve the following ℓ_0 optimisation problem:

$$\boldsymbol{\alpha}^\star = \underset{\boldsymbol{\alpha}}{\arg\min} \|\alpha\|_0 \text{ such that } \|\boldsymbol{y} - \Phi\Psi\boldsymbol{\alpha}\|_2 \leq \epsilon ,$$

  where the signal is synthesising by $\boldsymbol{x}^\star = \Psi \boldsymbol{\alpha}^\star$.

- Recall norms given by:

$$\|\alpha\|_0 = \text{no. non-zero elements} \qquad \|\alpha\|_1 = \sum_i |\alpha_i| \qquad \|\alpha\|_2 = \Big(\sum_i |\alpha_i|^2\Big)^{1/2}$$

- Solving this problem is difficult (combinatorial).

- Instead, solve the ℓ_1 optimisation problem (convex):

$$\boldsymbol{\alpha}^\star = \underset{\boldsymbol{\alpha}}{\arg\min} \|\alpha\|_1 \text{ such that } \|\boldsymbol{y} - \Phi\Psi\boldsymbol{\alpha}\|_2 \leq \epsilon .$$

An introduction to compressive sensing

- Ill-posed inverse problem:

$$\boldsymbol{y} = \Phi \boldsymbol{x} + \boldsymbol{n} = \Phi \Psi \boldsymbol{\alpha} + \boldsymbol{n} .$$

- Solve by imposing a regularising prior that the signal to be recovered is sparse in Ψ, *i.e.* solve the following ℓ_0 optimisation problem:

$$\boldsymbol{\alpha}^\star = \arg\min_{\boldsymbol{\alpha}} \|\alpha\|_0 \text{ such that } \|\boldsymbol{y} - \Phi\Psi\boldsymbol{\alpha}\|_2 \leq \epsilon ,$$

  where the signal is synthesising by $\boldsymbol{x}^\star = \Psi \boldsymbol{\alpha}^\star$.

- Recall norms given by:

$$\|\alpha\|_0 = \text{no. non-zero elements} \qquad \|\alpha\|_1 = \sum_i |\alpha_i| \qquad \|\alpha\|_2 = \Big(\sum_i |\alpha_i|^2\Big)^{1/2}$$

- Solving this problem is difficult (combinatorial).

- Instead, solve the ℓ_1 optimisation problem (convex):

$$\boldsymbol{\alpha}^\star = \arg\min_{\boldsymbol{\alpha}} \|\alpha\|_1 \text{ such that } \|\boldsymbol{y} - \Phi\Psi\boldsymbol{\alpha}\|_2 \leq \epsilon .$$

An introduction to compressive sensing

- The solutions of the ℓ_0 and ℓ_1 problems are often the same.

- Space of sparse vectors given by the union of subspaces aligned with the coordinate axes.

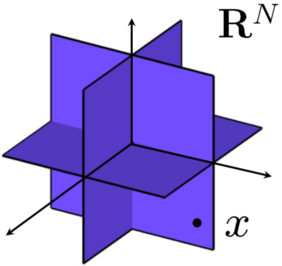

Figure: Space of the sparse vectors [Credit: Baraniuk]

An introduction to compressive sensing

- The solutions of the ℓ_0 and ℓ_1 problems are often the same.

- Restricted isometry property (RIP):

$$(1-\delta_{2K})\|\boldsymbol{x}_1-\boldsymbol{x}_2\|_2^2 \leq \|\Phi\boldsymbol{x}_1-\Phi\boldsymbol{x}_2\|_2^2 \leq (1+\delta_{2K})\|\boldsymbol{x}_!-\boldsymbol{x}_2\|_2^2 \,,$$

for K-sparse $\boldsymbol{x}$.

- Measurement must preserve geometry of sets of sparse vectors.

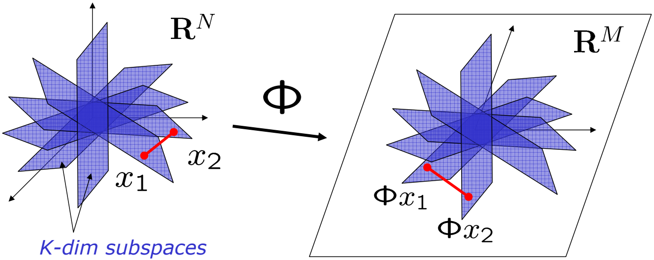

Figure: Measurement must preserve geometry of sets of sparse vectors. [Credit: Baraniuk]

An introduction to compressive sensing

- The solutions of the ℓ_0 and ℓ_1 problems are often the same.
- Geometry of ℓ_2 and ℓ_1 problems.

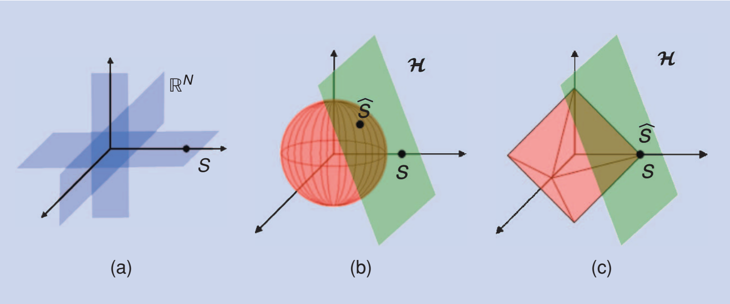

Figure: Geometry of (a) ℓ_0 (b) ℓ_2 and (c) ℓ_1 problems. [Credit: Baraniuk (2007)]

An introduction to compressive sensing

- In the absence of noise, compressed sensing is **exact!**
- Number of measurements required to achieve exact reconstruction is given by

$$M \geq c\mu^2 K \log N \, ,$$

where K is the sparsity and N the dimensionality.

- The coherence between the measurement and sparsity basis is given by

$$\mu = \sqrt{N} \max_{i,j} |\langle \Psi_i, \Phi_j \rangle| \, .$$

- Robust to noise.

An introduction to compressive sensing

- In the absence of noise, compressed sensing is **exact!**
- Number of measurements required to achieve exact reconstruction is given by

$$M \geq c\mu^2 K \log N \,,$$

where K is the sparsity and N the dimensionality.

- The coherence between the measurement and sparsity basis is given by

$$\mu = \sqrt{N} \max_{i,j} |\langle \Psi_i, \Phi_j \rangle| \,.$$

- Robust to noise.

An introduction to compressive sensing

- In the absence of noise, compressed sensing is **exact!**
- Number of measurements required to achieve exact reconstruction is given by

$$M \geq c\mu^2 K \log N \,,$$

where K is the sparsity and N the dimensionality.

- The coherence between the measurement and sparsity basis is given by

$$\mu = \sqrt{N} \max_{i,j} |\langle \Psi_i, \Phi_j \rangle| \,.$$

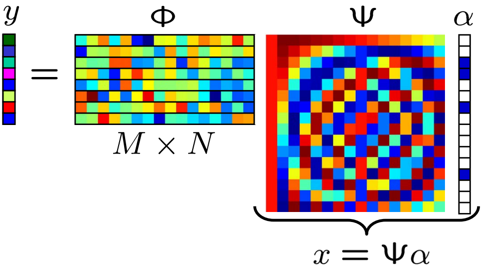

- Robust to noise.

An introduction to compressive sensing

- In the absence of noise, compressed sensing is **exact!**
- Number of measurements required to achieve exact reconstruction is given by

$$M \geq c\mu^2 K \log N \, ,$$

where K is the sparsity and N the dimensionality.

- The coherence between the measurement and sparsity basis is given by

$$\mu = \sqrt{N} \max_{i,j} |\langle \Psi_i, \Phi_j \rangle| \, .$$

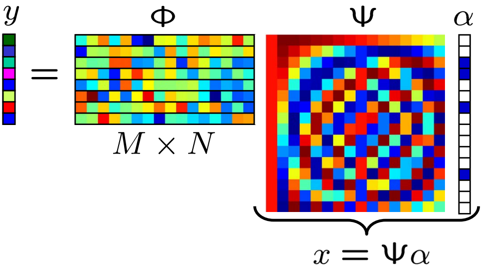

- Robust to noise.

Analysis-based approach

- Many new developments (*e.g.* analysis vs synthesis, cosparsity, structured sparsity).
- Typically sparsity assumption is justified by analysing example signals in terms of atoms of the dictionary.
- But this is different to synthesising signals from atoms.
- $\Rightarrow$ Analysis-based framework (Elad *et al.* 2007, Nam *et al.* 2012):

$$x^\star = \arg\min_{x} \|\Omega x\|_1 \text{ such that } \|y - \Phi x\|_2 \leq \epsilon \,.$$

- Contrast with synthesis-based approach:

$$x^\star = \Psi \cdot \arg\min_{\alpha} \|\alpha\|_1 \text{ such that } \|y - \Phi\Psi\alpha\|_2 \leq \epsilon \,.$$

- For orthogonal bases $\Omega = \Psi^\dagger$ and the two approaches are identical.

Analysis-based approach

- Many new developments (*e.g.* analysis vs synthesis, cosparsity, structured sparsity).
- Typically sparsity assumption is justified by analysing example signals in terms of atoms of the dictionary.
- But this is different to synthesising signals from atoms.
- $\Rightarrow$ Analysis-based framework (Elad *et al.* 2007, Nam *et al.* 2012):

$$x^\star = \arg\min_{x} \|\Omega x\|_1 \text{ such that } \|y - \Phi x\|_2 \leq \epsilon .$$

- Contrast with synthesis-based approach:

$$x^\star = \Psi \cdot \arg\min_{\alpha} \|\alpha\|_1 \text{ such that } \|y - \Phi\Psi\alpha\|_2 \leq \epsilon .$$

- For orthogonal bases $\Omega = \Psi^\dagger$ and the two approaches are identical.

Analysis-based approach

- Many new developments (*e.g.* analysis vs synthesis, cosparsity, structured sparsity).
- Typically sparsity assumption is justified by analysing example signals in terms of atoms of the dictionary.
- But this is different to synthesising signals from atoms.
- $\Rightarrow$ Analysis-based framework (Elad *et al.* 2007, Nam *et al.* 2012):

$$\boldsymbol{x}^\star = \arg\min_{\boldsymbol{x}} \|\Omega \boldsymbol{x}\|_1 \text{ such that } \|\boldsymbol{y} - \Phi \boldsymbol{x}\|_2 \leq \epsilon .$$

- Contrast with synthesis-based approach:

$$\boldsymbol{x}^\star = \Psi \cdot \arg\min_{\boldsymbol{\alpha}} \|\boldsymbol{\alpha}\|_1 \text{ such that } \|\boldsymbol{y} - \Phi \Psi \boldsymbol{\alpha}\|_2 \leq \epsilon .$$

- For orthogonal bases $\Omega = \Psi^\dagger$ and the two approaches are identical.

Analysis-based approach

- Many new developments (*e.g.* analysis vs synthesis, cosparsity, structured sparsity).
- Typically sparsity assumption is justified by analysing example signals in terms of atoms of the dictionary.
- But this is different to synthesising signals from atoms.
- $\Rightarrow$ Analysis-based framework (Elad *et al.* 2007, Nam *et al.* 2012):

$$\boldsymbol{x}^\star = \arg\min_{\boldsymbol{x}} \|\Omega \boldsymbol{x}\|_1 \text{ such that } \|\boldsymbol{y} - \Phi \boldsymbol{x}\|_2 \leq \epsilon \, .$$

- Contrast with synthesis-based approach:

$$\boldsymbol{x}^\star = \Psi \cdot \arg\min_{\boldsymbol{\alpha}} \|\boldsymbol{\alpha}\|_1 \text{ such that } \|\boldsymbol{y} - \Phi \Psi \boldsymbol{\alpha}\|_2 \leq \epsilon \, .$$

- For orthogonal bases $\Omega = \Psi^\dagger$ and the two approaches are identical.

Analysis-based approach

- For the case of redundant dictionaries, the analysis- and synthesis-based approaches are very different (Elad *et al.* 2007, Nam *et al.* 2012).

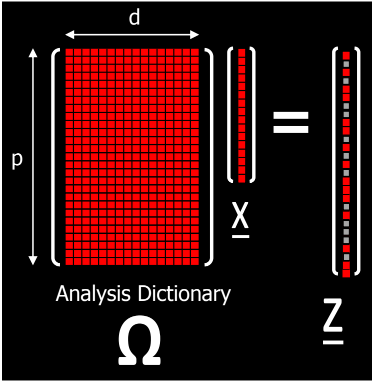

- Again, leads to a union of subspaces.
- But very different geometry to synthesis-based approach.

Analysis-based approach

- For a given redundancy, the size and number of subspaces is very different between the analysis- and synthesis-approaches (Nam *et al.* 2012).

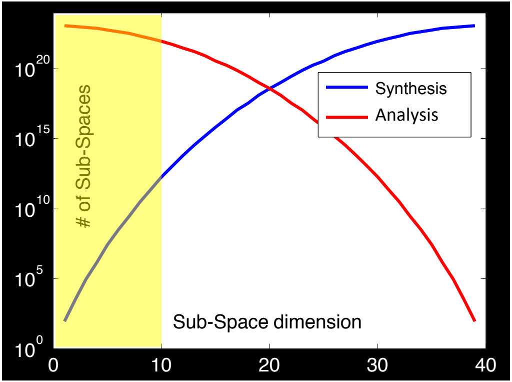

Comparison of analysis- and synthesis-based approaches

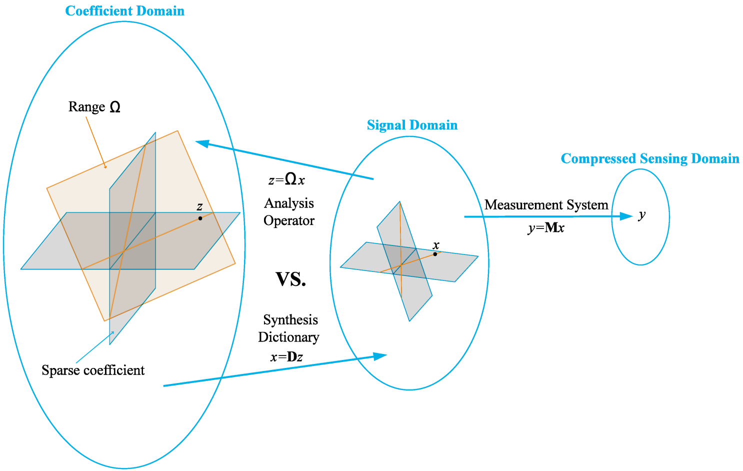

Figure: Analysis- and synthesis-based approaches [Credit: Nam *et al.* (2012)].

Comparison of analysis- and synthesis-based approaches

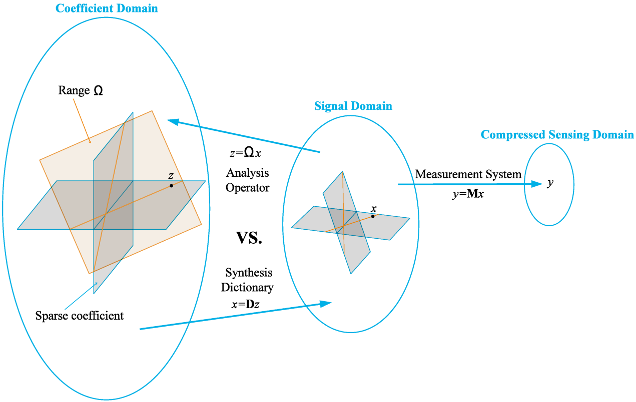

Figure: Analysis- and synthesis-based approaches [Credit: Nam *et al.* (2012)].

- Synthesis-based approach is more general, while analysis-based approach more restrictive.
- The more restrictive analysis-based approach may make it more robust to noise.
- The greater descriptive power of the synthesis-based approach may provide better signal representations.

A Bayesian perspective (synthesis-based approach)

- Consider the inverse problem:

$$\boldsymbol{y} = \Phi\Psi\boldsymbol{\alpha} + \boldsymbol{n} \; .$$

- Assume Gaussian noise, yielding the likelihood:

$$\mathrm{P}(\boldsymbol{y} \mid \boldsymbol{\alpha}) \propto \exp\Big(\|\boldsymbol{y} - \Phi\Psi\boldsymbol{\alpha}\|_2^2 / (2\sigma^2) \Big) \; .$$

- Consider the Laplacian prior:

$$\mathrm{P}(\boldsymbol{\alpha}) \propto \exp\Big(-\beta \|\boldsymbol{\alpha}\|_1 \Big) \; .$$

- The maximum *a-posteriori* (MAP) estimate is then

$$\boldsymbol{x}^\star_{\text{MAP-S}} = \Psi \cdot \underset{\boldsymbol{\alpha}}{\arg\max}\, \mathrm{P}(\boldsymbol{\alpha} \mid \boldsymbol{y}) = \Psi \cdot \underset{\boldsymbol{\alpha}}{\arg\min}\, \|\boldsymbol{y} - \Phi\Psi\boldsymbol{\alpha}\|_2^2 + \lambda \|\boldsymbol{\alpha}\|_1 \; ,$$

  with $\lambda = 2\beta\sigma^2$.

- One possible Bayesian interpretation.

- Recall also that the signal may not be distributed according to the prior but rather ℓ_0-sparse, in which case solving the ℓ_1 problem finds the correct ℓ_0-sparse solution.

A Bayesian perspective (synthesis-based approach)

- Consider the inverse problem:
$$y = \Phi\Psi\alpha + n \ .$$

- Assume Gaussian noise, yielding the likelihood:
$$\mathrm{P}(y \mid \alpha) \propto \exp\Big(\|y - \Phi\Psi\alpha\|_2^2/(2\sigma^2)\Big) \ .$$

- Consider the Laplacian prior:
$$\mathrm{P}(\alpha) \propto \exp\Big(-\beta\|\alpha\|_1\Big) \ .$$

- The maximum *a-posteriori* (MAP) estimate is then
$$x^\star_{\text{MAP-S}} = \Psi \cdot \underset{\alpha}{\arg\max}\ \mathrm{P}(\alpha \mid y) = \Psi \cdot \underset{\alpha}{\arg\min}\ \|y - \Phi\Psi\alpha\|_2^2 + \lambda\|\alpha\|_1 \ ,$$
with $\lambda = 2\beta\sigma^2$.

- One possible Bayesian interpretation.

- Recall also that the signal may not be distributed according to the prior but rather ℓ_0-sparse, in which case solving the ℓ_1 problem finds the correct ℓ_0-sparse solution.

A Bayesian perspective (synthesis-based approach)

- Consider the inverse problem:

$$\boldsymbol{y} = \Phi\Psi\boldsymbol{\alpha} + \boldsymbol{n} \ .$$

- Assume Gaussian noise, yielding the likelihood:

$$\mathrm{P}(\boldsymbol{y} \mid \boldsymbol{\alpha}) \propto \exp\Big(\|\boldsymbol{y} - \Phi\Psi\boldsymbol{\alpha}\|_2^2 / (2\sigma^2) \Big) \ .$$

- Consider the Laplacian prior:

$$\mathrm{P}(\boldsymbol{\alpha}) \propto \exp\Big(-\beta \|\boldsymbol{\alpha}\|_1 \Big) \ .$$

- The maximum *a-posteriori* (MAP) estimate is then

$$\boldsymbol{x}^{\star}_{\text{MAP-S}} = \Psi \cdot \underset{\boldsymbol{\alpha}}{\arg\max}\, \mathrm{P}(\boldsymbol{\alpha} \mid \boldsymbol{y}) = \Psi \cdot \underset{\boldsymbol{\alpha}}{\arg\min}\, \|\boldsymbol{y} - \Phi\Psi\boldsymbol{\alpha}\|_2^2 + \lambda \|\boldsymbol{\alpha}\|_1 \ ,$$

  with $\lambda = 2\beta\sigma^2$.

- One possible Bayesian interpretation.

- Recall also that the signal may not be distributed according to the prior but rather ℓ_0-sparse, in which case solving the ℓ_1 problem finds the correct ℓ_0-sparse solution.

Other Bayesian interpretations (synthesis-based approach)

- Other Bayesian interpretations of the synthesis-based approach are also possible (Gribonval 2011).
- Minimum mean square error (MMSE) estimators
  - $\subset$ synthesis-based estimators with appropriate penalty function, *i.e.* penalised least-squares (LS)
  - $\subset$ MAP estimators

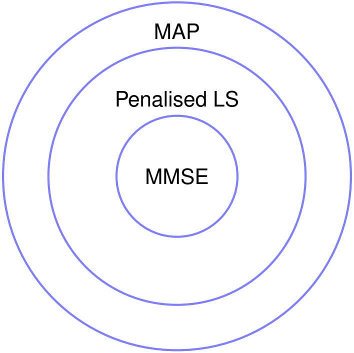

A Bayesian perspective (analysis-based approach)

- For the analysis-based approach, the MAP estimate is then

$$\boldsymbol{x}^{\star}_{\text{MAP-A}} = \arg\max_{\boldsymbol{x}} \mathrm{P}(\boldsymbol{x} \mid \boldsymbol{y}) = \arg\min_{\boldsymbol{x}} \|\boldsymbol{y} - \Phi\boldsymbol{x}\|_2^2 + \lambda\|\Omega\boldsymbol{x}\|_1 \ .$$

- Identical to the synthesis-based approach if $\Omega = \Psi^{\dagger}$.
- But for redundant dictionaries, the analysis-based MAP estimate is

$$\boldsymbol{x}^{\star}_{\text{MAP-A}} = \Omega^{\dagger} \cdot \arg\min_{\boldsymbol{\gamma} \in \text{column space } \Omega} \|\boldsymbol{y} - \Phi\Omega^{\dagger}\boldsymbol{\gamma}\|_2^2 + \lambda\|\boldsymbol{\gamma}\|_1 \ .$$

- Analysis- and synthesis-based approaches are quite different.
- Gain insight into the geometrical nature of problems (Elad *et al.* 2007, Nam *et al.* 2012).

A Bayesian perspective (analysis-based approach)

- For the analysis-based approach, the MAP estimate is then

$$\boldsymbol{x}^\star_{\text{MAP-A}} = \arg\max_{\boldsymbol{x}} \text{P}(\boldsymbol{x} \mid \boldsymbol{y}) = \arg\min_{\boldsymbol{x}} \|\boldsymbol{y} - \Phi\boldsymbol{x}\|_2^2 + \lambda \|\Omega\boldsymbol{x}\|_1 \ .$$

- Identical to the synthesis-based approach if $\Omega = \Psi^\dagger$.
- But for redundant dictionaries, the analysis-based MAP estimate is

$$\boldsymbol{x}^\star_{\text{MAP-A}} = \Omega^\dagger \cdot \arg\min_{\boldsymbol{\gamma} \in \text{column space } \Omega} \|\boldsymbol{y} - \Phi\Omega^\dagger\boldsymbol{\gamma}\|_2^2 + \lambda \|\boldsymbol{\gamma}\|_1 \ .$$

- Analysis- and synthesis-based approaches are quite different.
- Gain insight into the geometrical nature of problems (Elad *et al.* 2007, Nam *et al.* 2012).

A Bayesian perspective (analysis-based approach)

- For the analysis-based approach, the MAP estimate is then

$$\boldsymbol{x}^{\star}_{\text{MAP-A}} = \arg\max_{\boldsymbol{x}} \text{P}(\boldsymbol{x} \mid \boldsymbol{y}) = \arg\min_{\boldsymbol{x}} \|\boldsymbol{y} - \Phi\boldsymbol{x}\|_2^2 + \lambda\|\Omega\boldsymbol{x}\|_1 .$$

- Identical to the synthesis-based approach if $\Omega = \Psi^{\dagger}$.
- But for redundant dictionaries, the analysis-based MAP estimate is

$$\boldsymbol{x}^{\star}_{\text{MAP-A}} = \Omega^{\dagger} \cdot \arg\min_{\boldsymbol{\gamma} \in \text{column space } \Omega} \|\boldsymbol{y} - \Phi\Omega^{\dagger}\boldsymbol{\gamma}\|_2^2 + \lambda\|\boldsymbol{\gamma}\|_1 .$$

- Analysis- and synthesis-based approaches are quite different.
- Gain insight into the geometrical nature of problems (Elad *et al.* 2007, Nam *et al.* 2012).

Sparsity averaging and reweighting

- Sparsity averaging reweighted analysis (SARA) (Carrillo, McEwen & Wiaux 2012)
- Consider a dictionary composed of a concatenation of orthonormal bases, i.e.

$$\Psi = \frac{1}{\sqrt{q}}[\Psi_1, \Psi_2, \ldots, \Psi_q],$$

thus $\Psi \in \mathbb{R}^{N\times D}$ with $D = qN$.

- We consider the following bases:
  - Dirac, *i.e.* pixel basis
  - Haar wavelets (promotes gradient sparsity)
  - Daubechies wavelet bases two to eight.

$\Rightarrow$ concatenation of 9 bases

- Promote average sparsity by solving the reweighted ℓ_1 analysis problem:

$$\min_{\bar{x}\in\mathbb{R}^N} \|W\Psi^T\bar{x}\|_1 \quad \text{subject to} \quad \|y-\Phi\bar{x}\|_2 \leq \epsilon \quad \text{and} \quad \bar{x} \geq 0 \,,$$

where $W \in \mathbb{R}^{D\times D}$ is a diagonal matrix with positive weights.

- Solve a sequence of reweighted ℓ_1 problems using the solution of the previous problem as the inverse weights $\rightarrow$ approximate the ℓ_0 problem.

Sparsity averaging and reweighting

- Sparsity averaging reweighted analysis (SARA) (Carrillo, McEwen & Wiaux 2012)
- Consider a dictionary composed of a concatenation of orthonormal bases, i.e.

$$\Psi = \frac{1}{\sqrt{q}}[\Psi_1, \Psi_2, \ldots, \Psi_q],$$

  thus $\Psi \in \mathbb{R}^{N \times D}$ with $D = qN$.

- We consider the following bases:
  - Dirac, *i.e.* pixel basis
  - Haar wavelets (promotes gradient sparsity)
  - Daubechies wavelet bases two to eight.

  $\Rightarrow$ concatenation of 9 bases

- Promote average sparsity by solving the reweighted ℓ_1 analysis problem:

$$\min_{\bar{\boldsymbol{x}} \in \mathbb{R}^N} \|W \Psi^T \bar{\boldsymbol{x}}\|_1 \quad \text{subject to} \quad \|\boldsymbol{y} - \Phi \bar{\boldsymbol{x}}\|_2 \leq \epsilon \quad \text{and} \quad \bar{\boldsymbol{x}} \geq 0 \,,$$

  where $W \in \mathbb{R}^{D \times D}$ is a diagonal matrix with positive weights.

- Solve a sequence of reweighted ℓ_1 problems using the solution of the previous problem as the inverse weights $\rightarrow$ approximate the ℓ_0 problem.

SARA for radio interferometric imaging

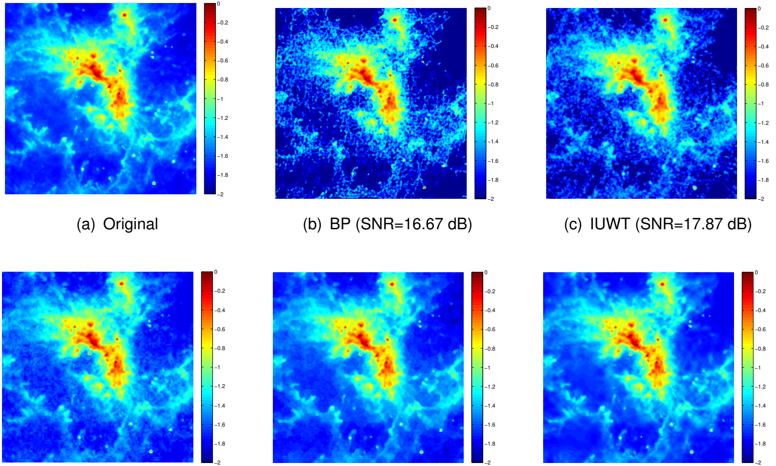

(a) Original (b) BP (SNR=16.67 dB) (c) IUWT (SNR=17.87 dB)

(d) BPDb8 (SNR=24.53 dB) (e) TV (SNR=26.47 dB) (f) SARA (SNR=29.08 dB)

Figure: Reconstruction example of 30Dor from 30% of visibilities.

SARA for radio interferometric imaging

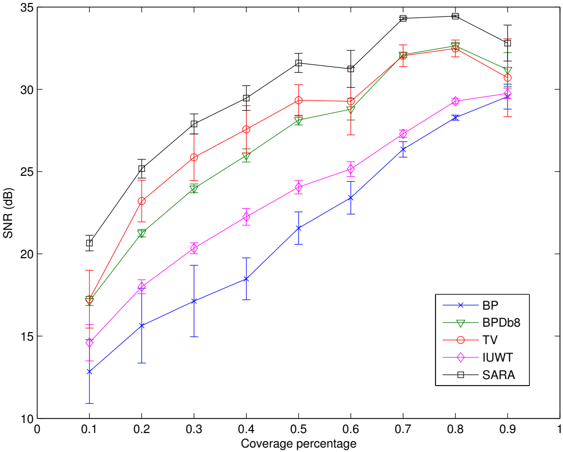

Figure: Reconstruction fidelity vs visibility coverage for 30Dor.

SARA for natural imaging

(a) Original (b) Daubechies 8 (c) SARA

Figure: Lena reconstruction from 30% of Fourier measurements.

SARA for natural imaging

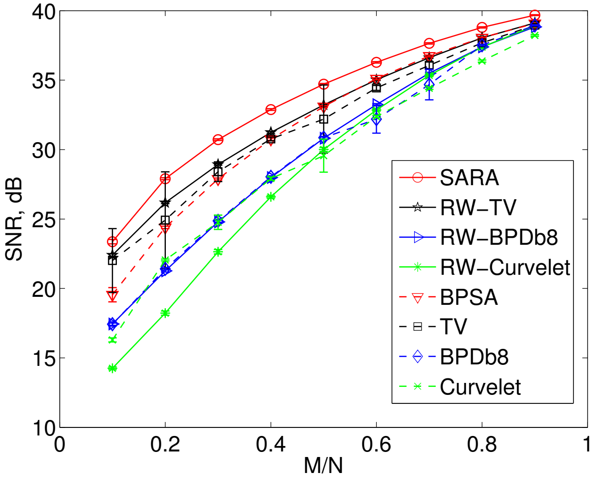

Figure: Reconstruction fidelity vs measurement ratio for Lena.

SARA for natural imaging

(a) Original

(b) Daubechies 8

(c) SARA

Figure: Cameraman reconstruction from 30% of Fourier measurements.

SARA for natural imaging

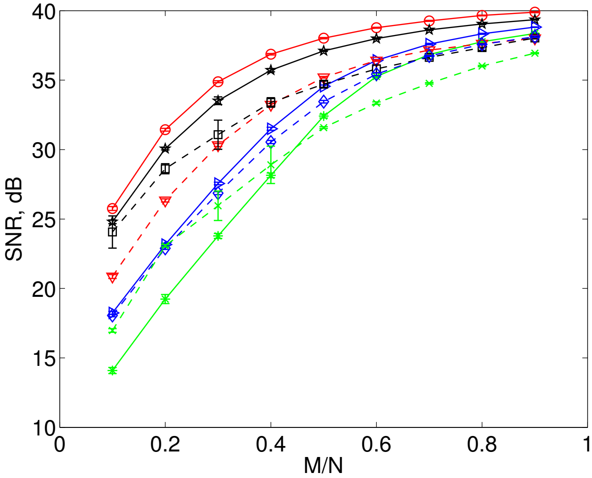

Figure: Reconstruction fidelity vs measurement ratio for Cameraman.

Sparse reconstruction on the sphere and ball

- We have been extending these ideas to the sphere and ball.

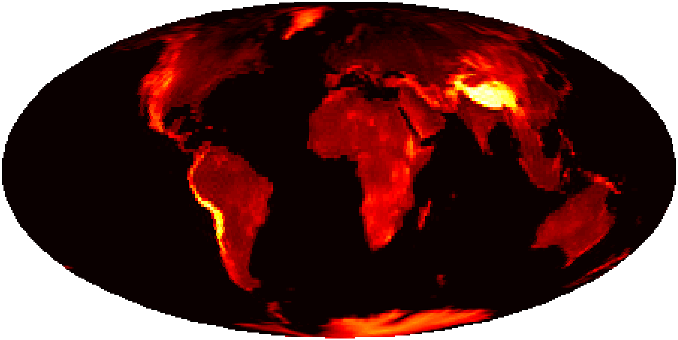

Figure: Ground truth at $L = 128$.

Sparse reconstruction on the sphere and ball

- We have been extending these ideas to the sphere and ball.

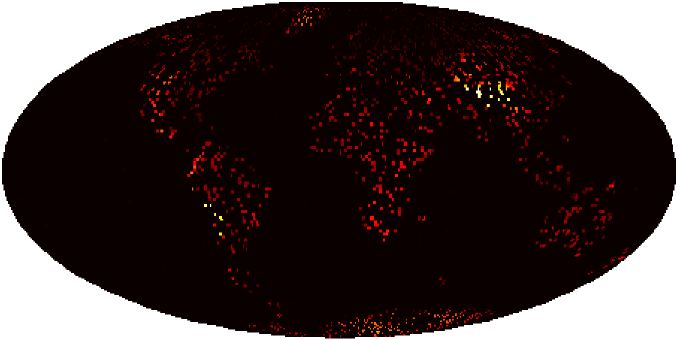

Figure: Measurements at $L = 128$ for $M/2L^2 = 1/8$.

Sparse reconstruction on the sphere and ball

- We have been extending these ideas to the sphere and ball.

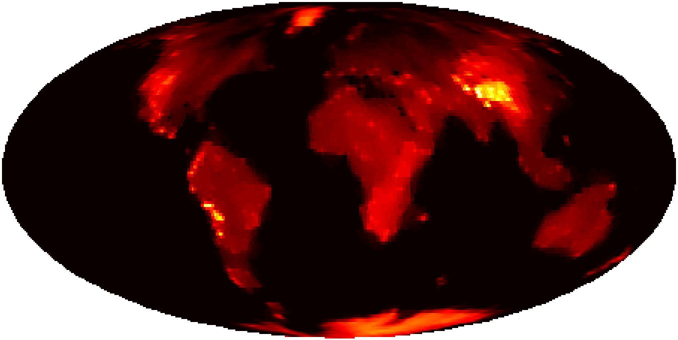

Figure: MW reconstruction in the harmonic domain at $L = 128$ for $M/2L^2 = 1/8$ ($\mathrm{SNR_I} = 20$dB).

Outline

CMB inpainting

- Incomplete observations of the CMB on the full-sky due to Galactic contamination.

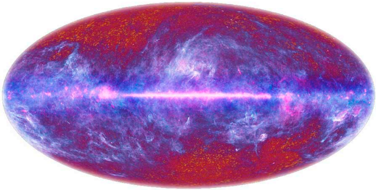

(a) Galactic contamination

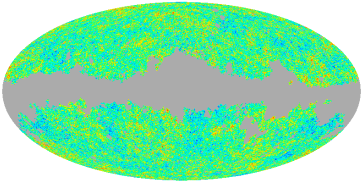

(b) Excise galaxy

- Model observations by $y = \Phi x = \Phi \Lambda \hat{x}$ where Λ represents the inverse spherical harmonic transform and $\hat{x}$ harmonic coefficients.
- Inpainting problem solved in harmonic space (Starck *et al.* 2012):

$$\hat{x}^\star = \underset{\hat{x}}{\arg\min} \, \|\hat{x}\|_1 \; \text{such that} \; y = \Phi \Lambda \hat{x} \, .$$

- Imposes sparsity of the spherical harmonic coefficients of the CMB!

CMB inpainting

- Incomplete observations of the CMB on the full-sky due to Galactic contamination.

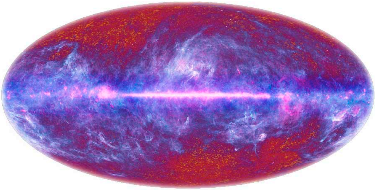

(a) Galactic contamination

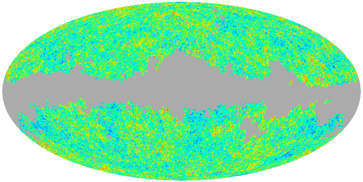

(b) Excise galaxy

- Model observations by $\boxed{y = \Phi x = \Phi \Lambda \hat{x}}$ where Λ represents the inverse spherical harmonic transform and $\hat{x}$ harmonic coefficients.
- Inpainting problem solved in harmonic space (Starck *et al.* 2012):

$$\boxed{\hat{x}^\star = \arg\min_{\hat{x}} \|\hat{x}\|_1 \ \text{such that}\ y = \Phi\Lambda\hat{x}\ .}$$

- Imposes sparsity of the spherical harmonic coefficients of the CMB!

CMB inpainting

- Incomplete observations of the CMB on the full-sky due to Galactic contamination.

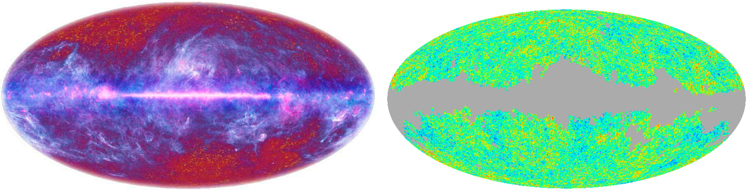

(a) Galactic contamination (b) Excise galaxy

- Model observations by $y = \Phi x = \Phi \Lambda \hat{x}$ where Λ represents the inverse spherical harmonic transform and $\hat{x}$ harmonic coefficients.
- Inpainting problem solved in harmonic space (Starck *et al.* 2012):

$$\hat{x}^\star = \underset{\hat{x}}{\arg\min} \, \|\hat{x}\|_1 \text{ such that } y = \Phi \Lambda \hat{x} .$$

- Imposes sparsity of the spherical harmonic coefficients of the CMB!

CMB inpainting

- **BUT** we have a very strong physical prior... the CMB is very close to Gaussian!
- Solving the CMB inpainting problem in this manner is equivalent to assuming harmonic coefficients are independent and Laplacian $\rightarrow$ not a good prior.
- Furthermore, for an isotropic random field, the harmonic coefficients are independent if and only if they are Gaussian distributed.
- We can see this intuitively since a rotation in harmonic space may be written

$$(\mathcal{R}(\alpha, \beta, \gamma)a)_{\ell m} = \sum_n D^{\ell}_{mn}(\alpha, \beta, \gamma)\, a_{\ell n} .$$

- Sparse CMB inpainting breaks statistical isotropy!

CMB inpainting

- **BUT** we have a very strong physical prior. . . the CMB is very close to Gaussian!
- Solving the CMB inpainting problem in this manner is equivalent to assuming harmonic coefficients are independent and Laplacian $\rightarrow$ not a good prior.
- Furthermore, for an isotropic random field, the harmonic coefficients are independent if and only if they are Gaussian distributed.
- We can see this intuitively since a rotation in harmonic space may be written

$$(\mathcal{R}(\alpha, \beta, \gamma)a)_{\ell m} = \sum_n D^{\ell}_{mn}(\alpha, \beta, \gamma)\, a_{\ell n}\ .$$

- Sparse CMB inpainting breaks statistical isotropy!

Cosmic strings

- Symmetry breaking phase transitions in the early Universe → topological defects.
- Cosmic strings well-motivated phenomenon that arise when axial or cylindrical symmetry is broken → line-like discontinuities in the fabric of the Universe.
- Although we have not yet observed cosmic strings, we have observed string-like topological defects in other media, e.g. ice and liquid crystal.
- Cosmic strings are distinct to the fundamental superstrings of string theory.
- However, recent developments in string theory suggest the existence of macroscopic superstrings that could play a similar role to cosmic strings.
- The detection of cosmic strings would open a new window into the physics of the Universe!

Figure: Optical microscope photograph of a thin film of freely suspended nematic liquid crystal after a temperature quench. [Credit: Chuang *et al.* (1991).]

Cosmic strings

- Symmetry breaking phase transitions in the early Universe → topological defects.
- Cosmic strings well-motivated phenomenon that arise when axial or cylindrical symmetry is broken → line-like discontinuities in the fabric of the Universe.
- Although we have not yet observed cosmic strings, we have observed string-like topological defects in other media, e.g. ice and liquid crystal.
- Cosmic strings are distinct to the fundamental superstrings of string theory.
- However, recent developments in string theory suggest the existence of macroscopic superstrings that could play a similar role to cosmic strings.
- The detection of cosmic strings would open a new window into the physics of the Universe!

Figure: Optical microscope photograph of a thin film of freely suspended nematic liquid crystal after a temperature quench. [Credit: Chuang *et al.* (1991).]

Cosmic strings

- Symmetry breaking phase transitions in the early Universe $\rightarrow$ topological defects.
- Cosmic strings well-motivated phenomenon that arise when axial or cylindrical symmetry is broken $\rightarrow$ line-like discontinuities in the fabric of the Universe.
- Although we have not yet observed cosmic strings, we have observed string-like topological defects in other media, e.g. ice and liquid crystal.
- Cosmic strings are distinct to the fundamental superstrings of string theory.
- However, recent developments in string theory suggest the existence of macroscopic superstrings that could play a similar role to cosmic strings.
- The detection of cosmic strings would open a new window into the physics of the Universe!

Figure: Optical microscope photograph of a thin film of freely suspended nematic liquid crystal after a temperature quench. [Credit: Chuang *et al.* (1991).]

Observational signatures of cosmic strings

- Spacetime about a cosmic string is canonical, with a three-dimensional wedge removed (Vilenkin 1981).
- Strings moving transverse to the line of sight induce line-like discontinuities in the CMB (Kaiser & Stebbins 1984).
- The amplitude of the induced contribution scales with $G\mu$, the string tension.

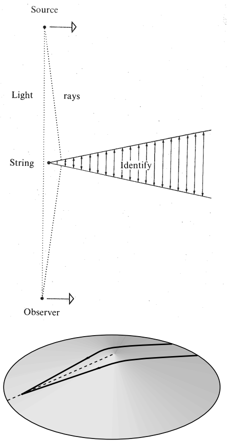

Spacetime around a cosmic string. [Credit: Kaiser & Stebbins 1984, DAMTP.]

Observational signatures of cosmic strings

- Make contact between theory and data using high-resolution simulations.
- Amplitude of the signal is given by the string tension $G\mu$.
- Search for a weak string signal s embedded in the CMB c, with observations d given by

$$d = c + s\ .$$

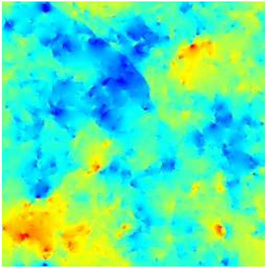

(a) Flat patch (Fraisse *et al.* 2008)

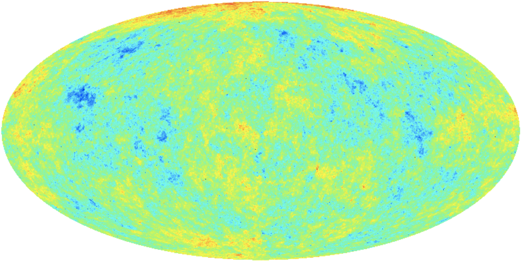

(b) Full-sky (Ringeval *et al.* 2012)

Figure: Cosmic string simulations.

Motivation for using wavelets to detect cosmic strings

- Adopt the scale-discretised wavelet transform on the sphere (Wiaux, McEwen *et al.* 2008), where we denote the wavelet coefficients of the data d by $\boxed{W^d_{j\rho} = \langle d,\ \Psi_{j\rho} \rangle}$ for scale $j \in \mathbb{Z}^+$ and position $\rho \in \mathrm{SO}(3)$.

- Consider an even azimuthal band-limit $N = 4$ to yield wavelet with odd azimuthal symmetry.

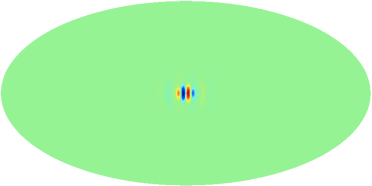

Figure: Example wavelet.

- Wavelet transform yields a sparse representation of the string signal $\rightarrow$ hope to effectively separate the CMB and string signal in wavelet space.

Motivation for using wavelets to detect cosmic strings

- Adopt the scale-discretised wavelet transform on the sphere (Wiaux, McEwen *et al.* 2008), where we denote the wavelet coefficients of the data d by $W^d_{j\rho} = \langle d, \Psi_{j\rho} \rangle$ for scale $j \in \mathbb{Z}^+$ and position $\rho \in \mathrm{SO}(3)$.
- Consider an even azimuthal band-limit $N = 4$ to yield wavelet with odd azimuthal symmetry.

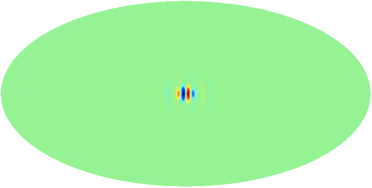

Figure: Example wavelet.

- Wavelet transform yields a sparse representation of the string signal $\rightarrow$ hope to effectively separate the CMB and string signal in wavelet space.

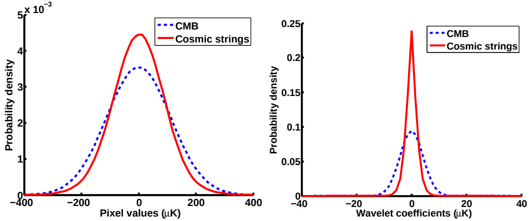

Figure: Distribution of CMB and string signal in pixel (left) and wavelet space (right).

Learning the statistics of the CMB and string signals in wavelet space

- Need to determine statistical description of the CMB and string signals in wavelet space.
- Calculate analytically the probability distribution of the CMB in wavelet space:

$$\mathrm{P}_j^c(W_{j\rho}^c) = \frac{1}{\sqrt{2\pi(\sigma_j^c)^2}} \mathrm{e}^{\left(-\frac{1}{2}\left(\frac{W_{j\rho}^c}{\sigma_j^c}\right)^2\right)} , \quad \text{where} \quad (\sigma_j^c)^2 = \langle W_{j\rho}^c \, W_{j\rho}^{c\,*} \rangle = \sum_{\ell m} C_\ell \left|(\Psi_j)_{\ell m}\right|^2 .$$

- Fit a generalised Gaussian distribution (GGD) for the wavelet coefficients of a string training map (*cf.* Wiaux *et al.* 2009):

$$\mathrm{P}_j^s(W_{j\rho}^s \mid G\mu) = \frac{\upsilon_j}{2G\mu\nu_j\Gamma(\upsilon_j^{-1})} \mathrm{e}^{\left(-\left|\frac{W_{j\rho}^s}{G\mu\nu_j}\right|^{\upsilon_j}\right)} ,$$

with scale parameter ν_j and shape parameter υ_j.

Learning the statistics of the CMB and string signals in wavelet space

- Need to determine statistical description of the CMB and string signals in wavelet space.
- Calculate analytically the probability distribution of the CMB in wavelet space:

$$\mathrm{P}_j^c(W_{j\rho}^c) = \frac{1}{\sqrt{2\pi(\sigma_j^c)^2}} \, \mathrm{e}^{\left(-\frac{1}{2}\left(\frac{W_{j\rho}^c}{\sigma_j^c}\right)^2\right)} , \quad \text{where} \quad (\sigma_j^c)^2 = \langle W_{j\rho}^c \, W_{j\rho}^{c\;*} \rangle = \sum_{\ell m} C_\ell \, |(\Psi_j)_{\ell m}|^2 \, .$$

- Fit a generalised Gaussian distribution (GGD) for the wavelet coefficients of a string training map (*cf.* Wiaux *et al.* 2009):

$$\mathrm{P}_j^s(W_{j\rho}^s \,|\, G\mu) = \frac{\upsilon_j}{2G\mu\nu_j\Gamma(\upsilon_j{}^{-1})} \, \mathrm{e}^{\left(-\left|\frac{W_{j\rho}^s}{G\mu\nu_j}\right|^{\upsilon_j}\right)} ,$$

with scale parameter ν_j and shape parameter υ_j.

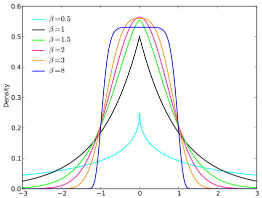

Figure: Generalised Gaussian distribution (GGD).

Learning the statistics of the CMB and string signals in wavelet space

- Require two simulated string maps: one for training; one for testing.

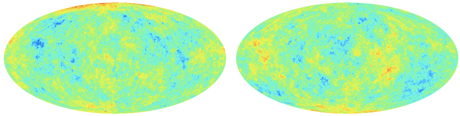

(a) String1 (b) String2

Figure: Cosmic string simulations.

- Compare distribution learnt from the training simulation (string2) with the distribution of the testing simulation (string1).
- Distributions in close agreement.

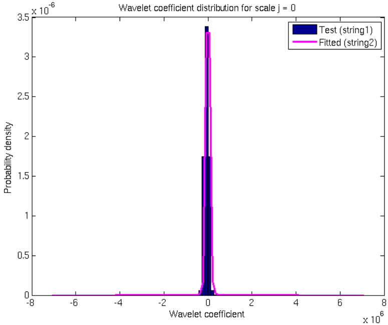

Figure: Distributions for wavelet scale $j = 0$.

Learning the statistics of the CMB and string signals in wavelet space

- Require two simulated string maps: one for training; one for testing.

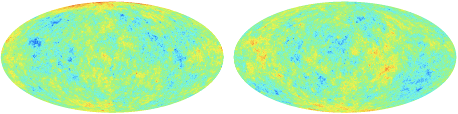

(a) String1 (b) String2

Figure: Cosmic string simulations.

- Compare distribution learnt from the training simulation (string2) with the distribution of the testing simulation (string1).
- Distributions in close agreement.

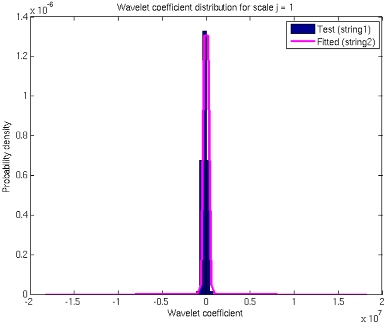

Figure: Distributions for wavelet scale $j = 1$.

Learning the statistics of the CMB and string signals in wavelet space

- Require two simulated string maps: one for training; one for testing.

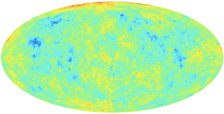

(a) String1

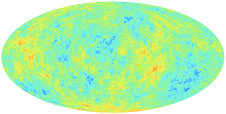

(b) String2

Figure: Cosmic string simulations.

- Compare distribution learnt from the training simulation (string2) with the distribution of the testing simulation (string1).
- Distributions in close agreement.

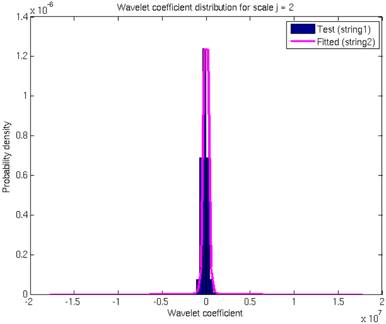

Figure: Distributions for wavelet scale $j = 2$.

Learning the statistics of the CMB and string signals in wavelet space

- Require two simulated string maps: one for training; one for testing.

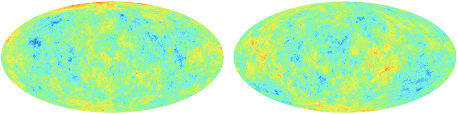

(a) String1 (b) String2

Figure: Cosmic string simulations.

- Compare distribution learnt from the training simulation (string2) with the distribution of the testing simulation (string1).
- Distributions in close agreement.

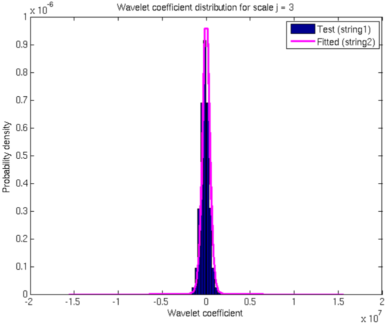

Figure: Distributions for wavelet scale $j = 3$.

Learning the statistics of the CMB and string signals in wavelet space

- Require two simulated string maps: one for training; one for testing.

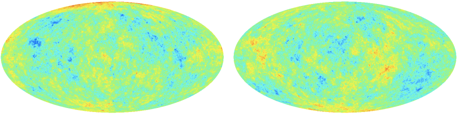

(a) String1 (b) String2

Figure: Cosmic string simulations.

- Compare distribution learnt from the training simulation (string2) with the distribution of the testing simulation (string1).
- Distributions in close agreement.

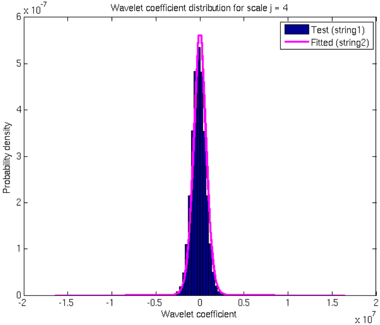

Figure: Distributions for wavelet scale $j = 4$.

Learning the statistics of the CMB and string signals in wavelet space

- Require two simulated string maps: one for training; one for testing.

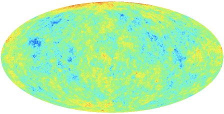

(a) String1

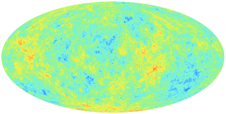

(b) String2

Figure: Cosmic string simulations.

- Compare distribution learnt from the training simulation (string2) with the distribution of the testing simulation (string1).
- Distributions in close agreement.
- We have accurately characterised the statistics of string signals in wavelet space.

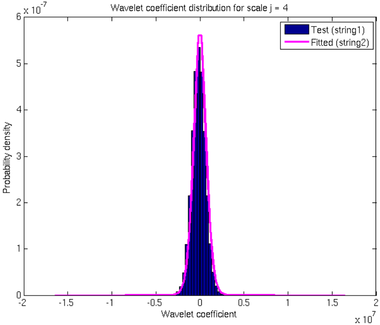

Figure: Distributions for wavelet scale $j = 4$.

Spherical wavelet-Bayesian string tension estimation

- Perform Bayesian string tension estimation in wavelet space, where the CMB and string distributions are very different.
- For each wavelet coefficient the likelihood is given by

$$\mathrm{P}(W^d_{j\rho} \mid G\mu) = \mathrm{P}(W^s_{j\rho} + W^c_{j\rho} \mid G\mu) = \int_{\mathbb{R}} \mathrm{d}W^s_{j\rho}\, \mathrm{P}^c_j(W^d_{j\rho} - W^s_{j\rho})\, \mathrm{P}^s_j(W^s_{j\rho} \mid G\mu)\,.$$

- The overall likelihood of the data is given by

$$\mathrm{P}(W^d \mid G\mu) = \prod_{j,\rho} \mathrm{P}(W^d_{j\rho} \mid G\mu)\,,$$

where we have assumed independence.

Spherical wavelet-Bayesian string tension estimation

- Perform Bayesian string tension estimation in wavelet space, where the CMB and string distributions are very different.

- For each wavelet coefficient the likelihood is given by

$$\mathrm{P}(W^d_{j\rho} \,|\, G\mu) = \mathrm{P}(W^s_{j\rho} + W^c_{j\rho} \,|\, G\mu) = \int_{\mathbb{R}} \mathrm{d}W^s_{j\rho} \; \mathrm{P}^c_j(W^d_{j\rho} - W^s_{j\rho}) \; \mathrm{P}^s_j(W^s_{j\rho} \,|\, G\mu) \; .$$

- The overall likelihood of the data is given by

$$\mathrm{P}(W^d \,|\, G\mu) = \prod_{j,\rho} \mathrm{P}(W^d_{j\rho} \,|\, G\mu) \; ,$$

where we have assumed independence.

Spherical wavelet-Bayesian string tension estimation

- Compute the string tension posterior $\mathrm{P}(G\mu \mid W^d)$ by Bayes theorem:

$$\mathrm{P}(G\mu \mid W^d) = \frac{\mathrm{P}(W^d \mid G\mu)\ \mathrm{P}(G\mu)}{\mathrm{P}(W^d)} \propto \mathrm{P}(W^d \mid G\mu)\ \mathrm{P}(G\mu)\ .$$

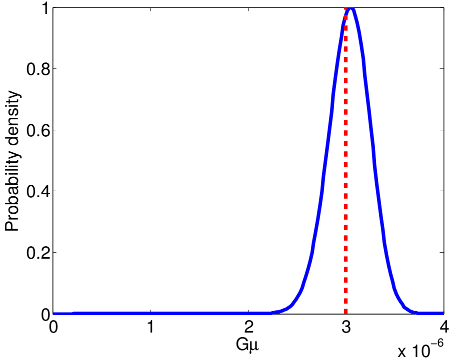

Figure: Posterior distribution of the string tension (true $G\mu = 3 \times 10^{-6}$).

Spherical wavelet-Bayesian string tension estimation

- Compute the string tension posterior $\mathrm{P}(G\mu \mid W^d)$ by Bayes theorem:

$$\mathrm{P}(G\mu \mid W^d) = \frac{\mathrm{P}(W^d \mid G\mu)\,\mathrm{P}(G\mu)}{\mathrm{P}(W^d)} \propto \mathrm{P}(W^d \mid G\mu)\,\mathrm{P}(G\mu)\,.$$

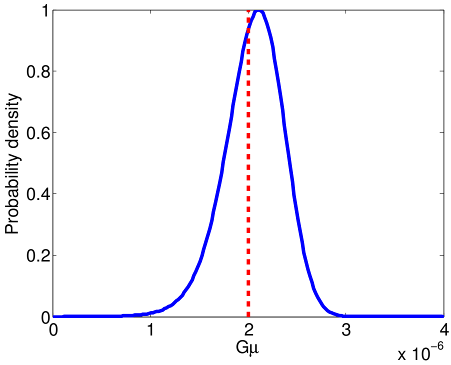

Figure: Posterior distribution of the string tension (true $G\mu = 2 \times 10^{-6}$).

Spherical wavelet-Bayesian string tension estimation

- Compute the string tension posterior $\text{P}(G\mu \mid W^d)$ by Bayes theorem:

$$\text{P}(G\mu \mid W^d) = \frac{\text{P}(W^d \mid G\mu)\,\text{P}(G\mu)}{\text{P}(W^d)} \propto \text{P}(W^d \mid G\mu)\,\text{P}(G\mu)\ .$$

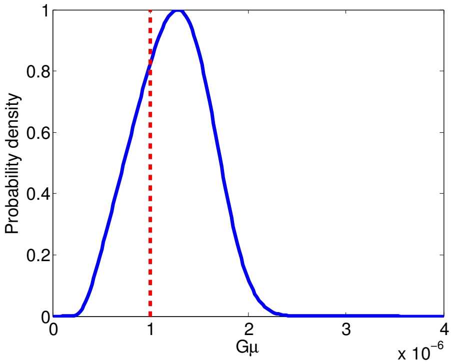

Figure: Posterior distribution of the string tension (true $G\mu = 1 \times 10^{-6}$).

Bayesian evidence for strings

- Compute Bayesian evidences to compare the string model M^s to the alternative model M^c that the observed data is comprised of just a CMB contribution.
- The Bayesian evidence of the string model is given by

$$E^s = \mathrm{P}(W^d \mid \mathrm{M}^s) = \int_{\mathbb{R}} \mathrm{d}(G\mu)\, \mathrm{P}(W^d \mid G\mu)\, \mathrm{P}(G\mu) \ .$$

- The Bayesian evidence of the CMB model is given by

$$E^c = \mathrm{P}(W^d \mid \mathrm{M}^c) = \prod_{j,\rho} \mathrm{P}^c_j(W^d_{j\rho}) \ .$$

- Compute the Bayes factor to determine the preferred model:

$$\Delta \ln E = \ln(E^s / E^c) \ .$$

Bayesian evidence for strings

- Compute Bayesian evidences to compare the string model M^s to the alternative model M^c that the observed data is comprised of just a CMB contribution.

- The Bayesian evidence of the string model is given by

$$E^s = \mathrm{P}(W^d \mid \mathrm{M}^s) = \int_{\mathbb{R}} \mathrm{d}(G\mu)\, \mathrm{P}(W^d \mid G\mu)\, \mathrm{P}(G\mu) \, .$$

- The Bayesian evidence of the CMB model is given by

$$E^c = \mathrm{P}(W^d \mid \mathrm{M}^c) = \prod_{j,\rho} \mathrm{P}_j^c(W_{j\rho}^d) \, .$$

- Compute the Bayes factor to determine the preferred model:

$$\Delta \ln E = \ln(E^s / E^c) \, .$$

Table: Tension estimates and log-evidence differences for simulations.

$G\mu/10^{-6}$	0.7	0.8	0.9	1.0	2.0	3.0
$\widehat{G\mu}/10^{-6}$	1.1	1.2	1.2	1.3	2.1	3.1
$\Delta \ln E$	-1.3	-1.1	-0.9	-0.7	5.5	29

Recovering string maps

- Our best inference of the underlying string map is encoded in the posterior probability distribution $\mathrm{P}(W^s_{j\rho} \mid W^d)$.

- Estimate the wavelet coefficients of the string map from the mean of the posterior distribution:

$$\overline{W}^s_{j\rho} = \int_{\mathbb{R}} \mathrm{d}W^s_{j\rho}\, W^s_{j\rho}\, \mathrm{P}(W^s_{j\rho} \mid W^d) = \int_{\mathbb{R}} \mathrm{d}(G\mu)\, \mathrm{P}(G\mu \mid d)\, \overline{W}^s_{j\rho}(G\mu) \,,$$

  where

$$\overline{W}^s_{j\rho}(G\mu) = \int_{\mathbb{R}} \mathrm{d}W^s_{j\rho}\, W^s_{j\rho}\, \mathrm{P}(W^s_{j\rho} \mid W^d_{j\rho}, G\mu) = \frac{1}{\mathrm{P}(W^d_{j\rho} \mid G\mu)} \int_{\mathbb{R}} \mathrm{d}W^s_{j\rho}\, W^s_{j\rho}\, \mathrm{P}^c_j(W^d_{j\rho} - W^s_{j\rho})\, \mathrm{P}^s_j(W^s_{j\rho} \mid G\mu) \,.$$

- Recover the string map from its wavelets (possible since the scale-discretised wavelet transform on the sphere supports exact reconstruction).

- Work in progress. . .

Recovering string maps

- Our best inference of the underlying string map is encoded in the posterior probability distribution $\mathrm{P}(W^s_{j\rho} \mid W^d)$.

- Estimate the wavelet coefficients of the string map from the mean of the posterior distribution:

$$\begin{aligned}\overline{W}^s_{j\rho} &= \int_{\mathbb{R}} \mathrm{d}W^s_{j\rho}\, W^s_{j\rho}\, \mathrm{P}(W^s_{j\rho} \mid W^d) \\ &= \int_{\mathbb{R}} \mathrm{d}(G\mu)\, \mathrm{P}(G\mu \mid d)\, \overline{W}^s_{j\rho}(G\mu)\ ,\end{aligned}$$

where

$$\begin{aligned}\overline{W}^s_{j\rho}(G\mu) &= \int_{\mathbb{R}} \mathrm{d}W^s_{j\rho}\, W^s_{j\rho}\, \mathrm{P}(W^s_{j\rho} \mid W^d_{j\rho}, G\mu) \\ &= \frac{1}{\mathrm{P}(W^d_{j\rho} \mid G\mu)} \int_{\mathbb{R}} \mathrm{d}W^s_{j\rho}\, W^s_{j\rho}\, \mathrm{P}^c_j(W^d_{j\rho} - W^s_{j\rho})\, \mathrm{P}^s_j(W^s_{j\rho} \mid G\mu)\ .\end{aligned}$$

- Recover the string map from its wavelets (possible since the scale-discretised wavelet transform on the sphere supports exact reconstruction).

- Work in progress. . .

Conclusions

Sparsity is a powerful concept that can provide new insight and is complementary to a Bayesian approach.

Conclusions

Sparsity is a powerful concept that can provide new insight and is complementary to a Bayesian approach.

But, as all techniques, sparsity must be exploited in the correct manner.

Just like in CosmoStats, in **Cosmo**Informatics the Cosmo is integral.

Extra slides on flaglet applications

Using flaglets to study large-scale structure (LSS)

- My flaglet decomposition of LSS provides a dual scale-spatial representation.

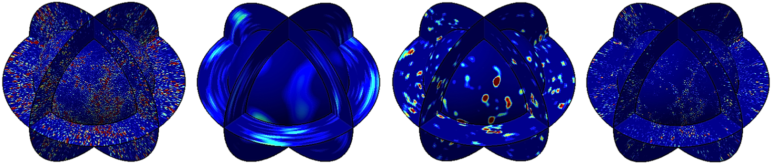

(a) Simulated LSS (b) Wavelet coefficients (large scale) (c) Wavelet coefficients (intermediate scale) (d) Wavelet coefficients (fine scale)

- Flaglets are a powerful analysis technique to handle systematics, noise and foregrounds.

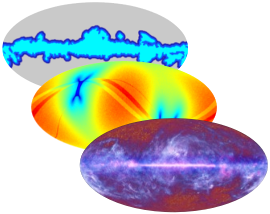

(a) Challenges for CMB analysis

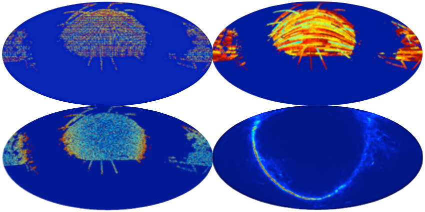

(b) Challenges for LSS analysis

Using flaglets to study large-scale structure (LSS)

- Flaglets are a powerful analysis technique to handle systematics, noise and foregrounds.

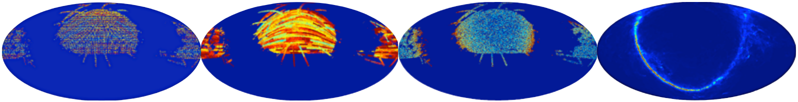

THEORY		THEORY + DATA		DATA
Fourier-Bessel space	→	*Flaglet space*	←	*Map space*
☺ Scale access		☺ Scale access		☹ No scale access
☹ Global in space		☺ Local in space		☺ Local in space

Extra slides on sparse recovery

Sparse signal reconstruction on the sphere

- Consider sparse reconstruction on the sphere.
- More efficient sampling theorem $\rightarrow$ implications for sparse signal reconstruction.
  - Improves both the dimensionality and sparsity signals in the spatial domain.
  - Improves the fidelity of sparse signal reconstruction.
- Consider the inverse problem

$$\boxed{\boldsymbol{y} = \Phi \boldsymbol{x} + \boldsymbol{n}}$$

where:
  - $\boldsymbol{x} \in \mathbb{R}^N$ denotes the samples of f;
  - N is the number of samples on the sphere of the adopted sampling theorem;
  - $\Phi \in \mathbb{R}^{M \times N}$ denotes the measurement operator, representing a random masking of the signal;
  - M noisy measurements $\boldsymbol{y} \in \mathbb{R}^M$ are acquired;
  - $\boldsymbol{n} \in \mathbb{R}^M$ denotes iid Gaussian noise with zero mean.

TV inpainting on the sphere

- Develop a framework for total variation (TV) inpainting on the sphere as illustrative example to study implications of sampling theorems (McEwen *et al.* 2013).

- Define TV norm on the sphere:

$$\int_{\mathbb{S}^2} \mathrm{d}\Omega \, |\nabla f| \simeq \sum_{t=0}^{N_\theta - 1} \sum_{p=0}^{N_\varphi - 1} |\nabla f| \, q(\theta_t) \simeq \sum_{t=0}^{N_\theta - 1} \sum_{p=0}^{N_\varphi - 1} \sqrt{q^2(\theta_t)(\delta_\theta \boldsymbol{x})^2 + \frac{q^2(\theta_t)}{\sin^2 \theta_t}(\delta_\varphi \boldsymbol{x})^2} \equiv \|\boldsymbol{x}\|_{\mathrm{TV},\mathbb{S}^2} \, .$$

- TV inpainting problem solved directly on the sphere:

$$\boldsymbol{x}^\star = \underset{\boldsymbol{x}}{\arg\min} \, \|\boldsymbol{x}\|_{\mathrm{TV},\mathbb{S}^2} \text{ such that } \|\boldsymbol{y} - \Phi \boldsymbol{x}\|_2 \leq \epsilon \, .$$

- TV inpainting problem solved in harmonic space:

$$\hat{\boldsymbol{x}}'^\star = \underset{\hat{\boldsymbol{x}}}{\arg\min} \, \|\Lambda \hat{\boldsymbol{x}}\|_{\mathrm{TV},\mathbb{S}^2} \text{ such that } \|\boldsymbol{y} - \Phi \Lambda \hat{\boldsymbol{x}}\|_2 \leq \epsilon \, ,$$

  where Λ represents the inverse spherical harmonic transform.

- Solve using convex optimisation techniques adapted to the sphere (Douglas-Rachford splitting).

TV inpainting: low-resolution simulations

- Solve TV inpainting problem on the sphere in the context of the Driscoll & Healy (1994) and the McEwen & Wiaux (2011) sampling theorems (at $L = 32$).

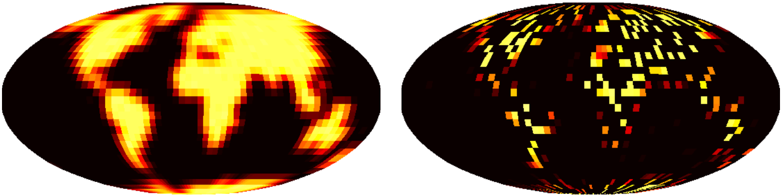

(a) Ground truth (b) Measurements

Figure: Earth topographic data reconstructed in the harmonic domain for $M/2L^2 = 1/4$

TV inpainting: low-resolution simulations

- Solve TV inpainting problem on the sphere in the context of the Driscoll & Healy (1994) and the McEwen & Wiaux (2011) sampling theorems (at $L = 32$).

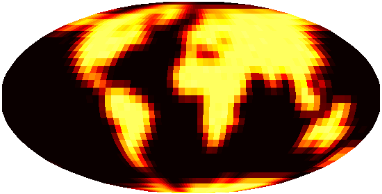

(a) Ground truth

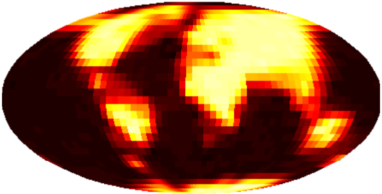

(b) DH reconstruction

Figure: Earth topographic data reconstructed in the harmonic domain for $M/2L^2 = 1/4$

TV inpainting: low-resolution simulations

- Solve TV inpainting problem on the sphere in the context of the Driscoll & Healy (1994) and the McEwen & Wiaux (2011) sampling theorems (at $L = 32$).

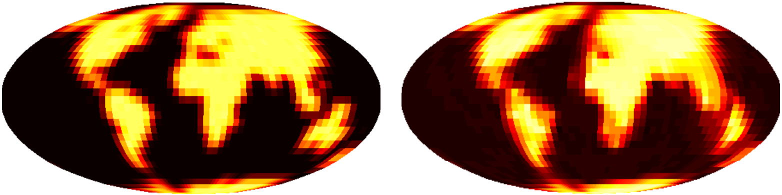

(a) Ground truth (b) MW reconstruction

Figure: Earth topographic data reconstructed in the harmonic domain for $M/2L^2 = 1/4$

TV inpainting: low-resolution simulations

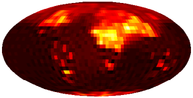

(a) DH spatial for $\frac{M}{L^2} = \frac{1}{4}$

(b) DH harmonic for $\frac{M}{L^2} = \frac{1}{4}$

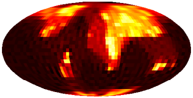

(c) MW spatial for $\frac{M}{L^2} = \frac{1}{4}$

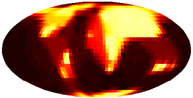

(d) MW harmonic for $\frac{M}{L^2} = \frac{1}{4}$

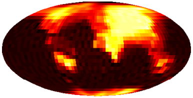

(e) DH spatial for $\frac{M}{L^2} = \frac{1}{2}$

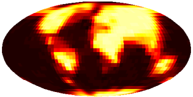

(f) DH harmonic for $\frac{M}{L^2} = \frac{1}{2}$

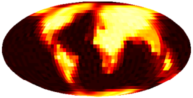

(g) MW spatial for $\frac{M}{L^2} = \frac{1}{2}$

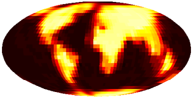

(h) MW harmonic for $\frac{M}{L^2} = \frac{1}{2}$

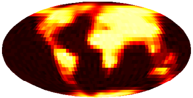

(i) DH spatial for $\frac{M}{L^2} = 1$

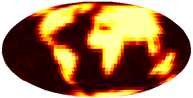

(j) DH harmonic for $\frac{M}{L^2} = 1$

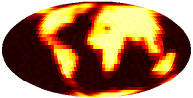

(k) MW spatial for $\frac{M}{L^2} = 1$

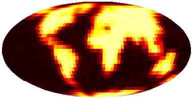

(l) MW harmonic for $\frac{M}{L^2} = 1$

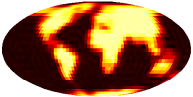

(m) DH spatial for $\frac{M}{L^2} = \frac{3}{2}$

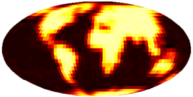

(n) DH harmonic for $\frac{M}{L^2} = \frac{3}{2}$

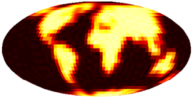

(o) MW spatial for $\frac{M}{L^2} = \frac{3}{2}$

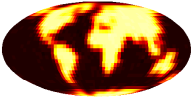

(p) MW harmonic for $\frac{M}{L^2} = \frac{3}{2}$

TV inpainting: low-resolution simulations

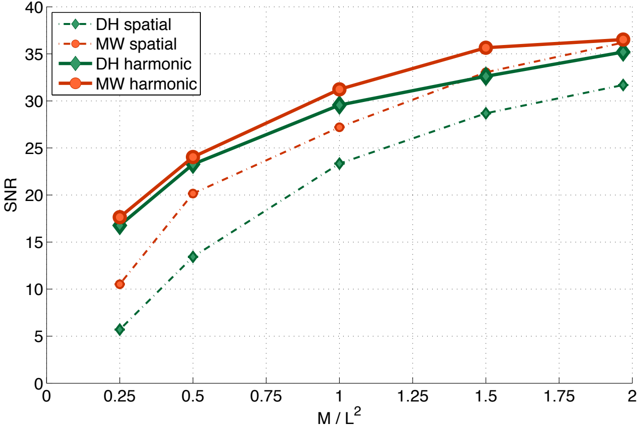

Figure: Reconstruction performance for the DH and MW sampling theorems

TV inpainting: high-resolution simulations

- Previously limited to low-resolution simulations.
- To solve high-resolution problem we require fast adjoint spherical harmonic transform operators in addition to fast forward spherical harmonic transforms to solve optimisation problems.
- Develop fast adjoints for the McEwen & Wiaux (2011) sampling theorem only.

Fast adjoint inverse spherical harmonic transform

$$ {}_s\tilde{f}^{\dagger}(\theta_t, \varphi_p) = \begin{cases} {}_sf(\theta_t, \varphi_p)\,, & t \in \{0, 1, \dots, L-1\} \\ 0\,, & t \in \{L, \dots, 2L-2\} \end{cases} $$

$$ {}_sF_{mm'}{}^{\dagger} = \sum_{t=0}^{2L-2} \sum_{p=0}^{2L-2} {}_s\tilde{f}^{\dagger}(\theta_t, \varphi_p)\, \mathrm{e}^{-\mathrm{i}(m'\theta_t + m\varphi_p)} $$

$$ {}_sf_{\ell m}{}^{\dagger} = (-1)^s\, \mathrm{i}^{m+s} \sqrt{\frac{2\ell+1}{4\pi}} \sum_{m'=-(L-1)}^{L-1} \Delta^{\ell}_{m'm}\, \Delta^{\ell}_{m',-s}\, {}_sF_{mm'}{}^{\dagger} $$

TV inpainting: high-resolution simulations

Fast adjoint forward spherical harmonic transform

$$ {}_sG_{mm'}{}^{\dagger} = (-1)^s \, \mathrm{i}^{-(m+s)} \sum_{\ell=0}^{L-1} \sqrt{\frac{2\ell+1}{4\pi}} \, \Delta^{\ell}_{m'm} \, \Delta^{\ell}_{m',-s} \, {}_sf_{\ell m} $$

$$ {}_sF_{mm''}{}^{\dagger} = 2\pi \sum_{m'=-(L-1)}^{L-1} {}_sG_{mm'}{}^{\dagger} \, w(m'-m'') $$

$$ {}_s\tilde{F}_m{}^{\dagger}(\theta_t) = \frac{1}{2L-1} \sum_{m'=-(L-1)}^{L-1} {}_sF_{mm'}{}^{\dagger} \, \mathrm{e}^{\mathrm{i}m'\theta_t} $$

$$ {}_sF_m{}^{\dagger}(\theta_t) = \begin{cases} {}_s\tilde{F}_m{}^{\dagger}(\theta_t) + (-1)^{m+s} \, {}_s\tilde{F}_m{}^{\dagger}(\theta_{2L-2-t}) \, , & t \in \{0, 1, \dots, L-2\} \\ {}_s\tilde{F}_m{}^{\dagger}(\theta_t) \, , & t = L-1 \end{cases} $$

$$ {}_sf^{\dagger}(\theta_t, \varphi_p) = \frac{1}{2L-1} \sum_{m=-(L-1)}^{L-1} {}_sF_m{}^{\dagger}(\theta_t) \, \mathrm{e}^{\mathrm{i}m\varphi_p} $$

TV inpainting: high-resolution simulations

- Using fast adjoints we solve high-resolution TV inpainting problem with realistic data.

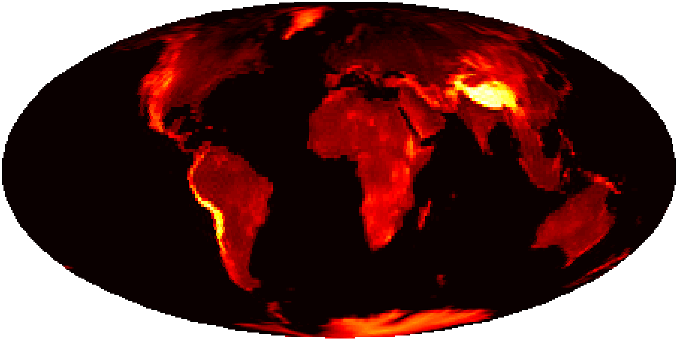

Figure: Ground truth at $L = 128$.

TV inpainting: high-resolution simulations

- Using fast adjoints we solve high-resolution TV inpainting problem with realistic data.

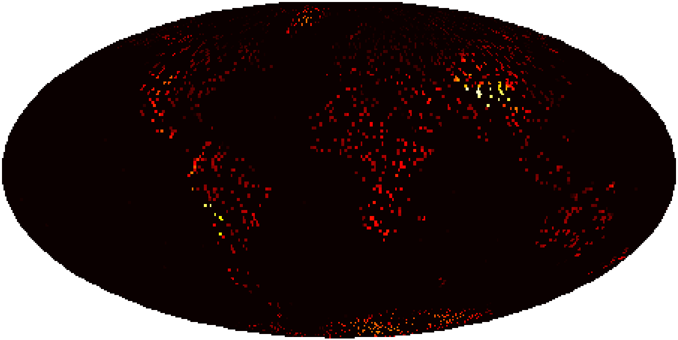

Figure: Measurements at $L = 128$ for $M/2L^2 = 1/8$.

TV inpainting: high-resolution simulations

- Using fast adjoints we solve high-resolution TV inpainting problem with realistic data.

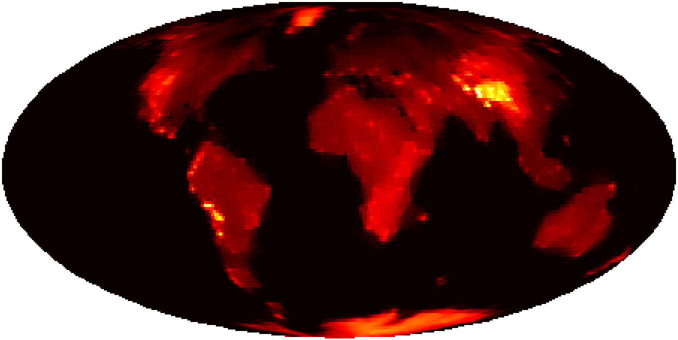

Figure: MW reconstruction in the harmonic domain at $L = 128$ for $M/2L^2 = 1/8$ ($\mathrm{SNR_I} = 20$dB).